To be submitted to Economic Geology

Geological and chronological constraints on the long-lived Eocene Yulong porphyry Cu-Mo deposit, eastern Tibet, China: implications for lifespan of magmatic-hydrothermal processes forming giant and supergiant porphyry Cu deposits

JIA CHANG,[1,2] JIAN-WEI LI,[1,2*] DAVID SELBY,[3] JIA-CHENG LIU,[2] XIAO-DONG DENG[1]

[1] State Key Laboratory of Geological Processes and Mineral Resources, China University of Geosciences, Wuhan 430074, China

[2] Faculty of Earth Resources, China University of Geosciences, Wuhan 430074, China

[3] Department of Earth Sciences, Durham University, DH1 3LE Durham, UK

* Corresponding author:

E-mail: jwli@cug.edu.cn

Phone: +86 138 7111 2076

Fax: +86 27 6788 5096

Abstract

The Yulong porphyry Cu-Mo deposit, the third largest porphyry Cu deposit in China, contains proven reserves of >6.5 Mt Cu and 0.4 Mt Mo. Previous radiometric dating studies have provided numerous ages for this deposit, but the timing and duration of the process governing the deposition of Cu and Mo remains not well constrained. In this paper, we first document multiple stages of mineralization and hydrothermal alteration associated with distinct magmatic pulses at Yulong by field and textural relationships, and then present high-precision molybdenite Re-Os ages of 14 quartz-molybdenite ± chalcopyrite veins representing these stages to precisely constrain the timing and duration of Cu-Mo mineralization.

The ore-hosting Yulong composite stock consists of three successive porphyry intrusions: (1) monzonitic granite porphyry (MGP), (2) K-feldspar granite porphyry (KGP), and (3) quartz albite porphyry (QAP). The vein formation, Cu-Mo mineralization and ore-related alteration are grouped into early, transitional and late stages with respect to the intrusive history. The first two porphyry intrusions are followed by cyclical sequences of veining that are mainly associated with potassic alteration and have formed (1) M_E vein/UST_T, (2) $EB_{E/T}$ veins, (3) $A1_{E/T}$ veins, (4) $A2_E/B_T$ veins, and (5) $A3_{E/T}$ veins. $A2_E/B_T$ and $A3_{E/T}$ veins of the early and transitional stages are dominated by quartz and chalcopyrite ± pyrite, respectively, and represent the main Cu-Mo mineralization events. More than 80 % of Cu and Mo at Yulong were deposited in the early stage with the remainder being formed in the transitional stage. The late stage pyrite-quartz veins (D_L), which are characterized by sericitic alteration halos, postdate the intrusion of QAP dikes and have no economic significance.

Molybdenite Re-Os ages of $A2_E$ and B_T veins indicate that sulfide deposition at Yulong was episodic over a prolonged history lasting over 5.13 ± 0.23 m.y. (1σ). However, the bulk Cu-Mo ores formed in a shorter time interval of 1.36 ± 0.24 m.y. (1σ) with most Cu precipitated in a more restricted timespan of 0.82 ± 0.24 m.y. (1σ) in the early stage. These results, combined with geochronologic data from porphyry

copper deposits elsewhere, confirm that multiple magmatic-hydrothermal pulses with a lifespan of tens to hundreds of thousands of years are sufficient to form a giant porphyry copper deposit. Factors such as metal concentration, volume and focusing efficiency of ore-forming fluids could have played important roles in producing a giant porphyry Cu deposit regardless of a short- or long-lived magmatic-hydrothermal system.

Introduction

Porphyry Cu-(Mo-Au) deposits (PCDs), commonly developed above large upper crustal magma chambers (Sillitoe, 2010), represent focused zones of intrusive activity, heat transfer, fluid-flow, mineral precipitation, and hydrothermal alteration of great economic significance. Knowledge on the timing and duration of magmatic-hydrothermal processes is of critical importance to better understand the formation and evolution of PCDs (Chiaradia et al., 2013). Previous studies have shown that many large porphyry systems are products of multiple magmatic-hydrothermal pulses spanning periods of less than one to a few million years (Sillitoe and Mortensen, 2010; von Quadt et al., 2011; Braxton et al., 2012; Stein, 2014; Spencer et al., 2015; Buret et al., 2016). The maximum lifespan of an individual magmatic-hydrothermal pulse, however, may last only a few to tens of thousands of years (Cathles et al., 1997; Simmons and Brown, 2006; Weis et al., 2012).

Recent technical development has allowed dating of minerals using U-Pb, $^{40}Ar/^{39}Ar$ and Re-Os systems at internal precisions sufficient to resolve events at the hundred to ten thousand years scale in young porphyry deposits (Chiaradia et al., 2013). Zircon U-Pb dating of pre-, syn- and post-ore porphyry phases can only indirectly bracket the maximum lifespan of the magmatic-hydrothermal events (Sillitoe and Mortensen, 2010; von Quadt et al., 2011; Buret et al., 2016), whereas $^{40}Ar/^{39}Ar$ dating of K-bearing minerals with relatively low closure temperatures for argon isotopes does not necessarily measure the ages of magma intrusions or early

high-temperature hydrothermal alteration events in the porphyry environment (Maksaev et al., 2004; Harris et al., 2008; Deckart et al., 2012). In contrast, molybdenite Re-Os dating has been proven to be a robust chronometer and commonly provides direct and reliable constraints on the timing and evolution of porphyry systems as recorded in multiple molybdenite-bearing vein assemblages spanning the entire duration of the porphyry copper mineralization process, with the results defining repeated events in absolute time and the lifespan of porphyry systems (Maksaev et al., 2004; Deckart et al., 2012; Stein, 2014; Spencer et al., 2015; Li et al., in press).

Extensive studies have been done on characteristics and genesis of the Yulong porphyry Cu-Mo deposit since its discovery in the 1960s (Du, 1985; Tang et al., 1995; Hou et al., 2003, 2006; Liang et al., 2006, 2009; Li et al., 2012). Nevertheless, the chronology of Cu-Mo mineralization relative to the intrusive sequence, different vein types and hydrothermal alteration assemblages has not been well established. This is largely due to that the uppermost zone of the deposit has suffered from intensive oxidization and supergene kaolinite leaching that have obscured the relative chronological relations of magmatic and hydrothermal events, and to the fact that early exploration drill holes have rarely reached the deep and relatively well-preserved mineralization zone. In the last decade, a large number of new drill holes penetrating the entire ore zone have made it possible to establish the spatial and temporal relationships of porphyry intrusions, vein formation, hydrothermal alteration, and Cu-Mo mineralization.

Our detailed drill core logging results suggest that the deposit consists of cyclical formation of quartz-molybdenite ± chalcopyrite veins that record multiple pulses of Cu-Mo mineralization. These veins provide an excellent opportunity to determine the absolute timing and duration of magmatic-hydrothermal activities at Yulong by using molybdenite Re-Os dating. The Re-Os dates are interpreted in the context of intrusive ages of different porphyry phases constrained by U-Pb zircon geochronology carried out with laser ablation inductively-coupled plasma mass spectrometry (LA-ICP-MS). Geological, petrographic and geochronological results presented here are used to gain

insights into the evolution of the Yulong deposit. Combined with the existing high-precision geochronologic data of PCDs elsewhere, this study also allows a better understanding in the lifetime of magmatic-hydrothermal systems responsible for a giant PCD.

Geologic Background

The Yulong porphyry copper belt, 15-30 km wide and ~300 km long, is situated in the Changdu-Simao continental block along the eastern margin of the Tibet Plateau (Fig. 1A; Hou et al., 2003). The Changdu-Simao block is bordered by several Cenozoic strike-slip and pull-apart basins, and consists of poorly exposed Proterozoic crystalline basement and early Paleozoic folded basement, thick middle Paleozoic to late Mesozoic marine carbonate, clastic and volcanic rocks, and a Cenozoic red molasse sequences intercalated with alkaline volcanic rocks that have whole-rock, K-feldspar and biotite K-Ar ages of 43 to 38 Ma (Hou et al., 2003 and references therein). More than 100 Eocene porphyry intrusions were emplaced into the block between 55 and 34 Ma, based on Rb-Sr dating of whole-rock samples, K-Ar dating of igneous biotite and LA-ICP-MS or SHRIMP U-Pb dating of igneous zircons (Ma, 1990; Tang and Luo, 1995; Hou et al., 2003; Liang et al., 2006). The emplacement and distribution of the Eocene volcanic rocks and porphyry intrusions are considered to be controlled by the north-south to north-northwest, regional strike-slip faults, which formed during the India-Asian continental collision (Hou et al., 2003). Five major porphyry Cu-(Mo) deposits in the Yulong copper belt are closely associated with the Eocene porphyry intrusions, which have LA-ICP-MS zircon U-Pb ages ranging from 41.2 ± 0.2 Ma to 36.9 ± 0.4 Ma (Liang et al., 2006).

The Yulong porphyry Cu-Mo deposit, the largest one in the Yulong porphyry copper belt, has proven reserves of > 6.5 Mt Cu at 0.62 % and >0.4 Mt Mo at 0.042 % (Tibet Yulong Copper Co., Ltd., 2009). The deposit is centered on a composite porphyry stock that intruded a sequence of Triassic marine clastic and carbonate rocks at the southern end of the north- to northwest-trending Hengxingcuo anticline (Fig.

1B), which provided a structural control for the emplacement and distribution of more than 40 porphyry intrusions. The ore zone in the Yulong porphyry stock and, less significantly, the proximal hornfels has an asymmetric, inverted cup-like shape in three dimensions (Fig. 2), with the highest economic ore grades occurring in the southeastern part of the deposit extending downward to 4000 m a.s.l. The ore zone encloses a sub-economic to barren core (<0.3 wt% Cu), the top of which is about 4300-4400 m in elevation in the center of the stock. The grades of Cu and Mo mineralization correlate closely above ~4300 m a.s.l., with the Mo/Cu ratio increasing with depth. In addition, a significant amount of Cu ores occur within skarn assemblages at the contact between the stock and upper Triassic marine limestones. Detailed description of the skarn alteration and mineralization was given in Tang et al. (1995). Both the skarn and porphyry type mineralization have been exposed to the surface and extensively oxidized, leading to significant supergene copper enrichment (Tang, 2003). The supergene Cu mineralization in the shallow porphyry ore is largely manifested by variable replacement of chalcopyrite with covellite and chalcocite. Recent goethite (U-Th)/He dating has revealed a prolonged history of oxidation and supergene mineralization between 6.73 ± 0.51 and 0.53 ± 0.04 Ma (2σ; Deng et al., 2017).

Previous Geochronological Studies at Yulong

Published geochronological data for the Yulong Cu-Mo deposit and two nearby barren porphyry intrusions, which were probably sourced from the same deep-seated magma chamber as the Yulong stock, are summarized in Figure 3. K/Ar or Rb-Sr isochron dating of magmatic biotite and K-feldspar from the monzonitic granite porphyry (MGP) yielded dates ranging from 55 to 38 Ma with analytical uncertainty up to ± 8% (Ma, 1990). The geological significance of these ages is questionable considering (1) the low closure temperatures of the K-Ar and Rb-Sr isotope systems in biotite and K-feldspar, and (2) the repeated magmatic/hydrothermal events in the Yulong deposit that may have disturbed or reset the biotite and K-feldspar K-Ar and

Rb-Sr isotope systematics. Recent zircon U-Pb geochronology studies (Guo et al., 2006; Liang et al., 2006; Li et al., 2012) yielded internally reproducible age results for the MGP of 41.2 ± 1.5 Ma (1σ), 41.02 ± 0.24 Ma (2σ) and 40.89 ± 0.17 Ma (2σ). However, a slightly older SHRIMP zircon U-Pb age of 43.0 ± 0.5 Ma (2σ) for the MGP is reported by Wang et al. (2009). This age difference reflects either truly different zircon populations, differences in analytical techniques (SHRIMP vs. LA-ICP-MS) or different experimental protocols (von Quadt et al., 2011; Chiaradia et al., 2013; Schaltegger et al., 2015).

Previous $^{40}Ar/^{39}Ar$ dating of hydrothermal biotite from the potassic alteration zone yielded a poorly-defined plateau age of 41.3 ± 0.8 Ma (Liang et al., 2008). Neither analytical results nor discussion of the validity of the $^{40}Ar/^{39}Ar$ age was given in Liang et al. (2008), thus the significance of this date is unclear. The age of Cu-Mo mineralization at Yulong has been constrained by ID-ICPMS molybdenite Re-Os dating, with results ranging from 41.29 ± 0.56 to 39.69 ± 0.57 Ma (2σ) (Hou et al., 2006; Tang et al., 2009). These ages may indicate prolonged and likely multistage Cu-Mo mineralization, but the analytical precision inherent with the ICP-MS analysis (1.4-2.0 %) and the unclear field-based chronology of the dated molybdenite-bearing quartz veins cast doubt on the lifetime of the magmatic-hydrothermal system.

In a recent study, five (U-Th)/He zircon ages for the MGP, which are between 35.7 ± 1.2 and 39.6 ± 1.4 Ma (2σ), were combined with the above-mentioned zircon U-Pb dating results to suggest a relatively long-lived magmatic-hydrothermal system lasting at least ~5 m.y. (Li et al., 2012). Because zircon (U-Th)/He ages represent the time of cooling of the system below 200 °C (Reiners, 2005), their significance in determining the duration of mineralization and alteration is questionable. Li et al. (2012) also obtained four (U-Th)/He apatite ages from 32.7 ± 1.2 to 34.3 ± 1.0 Ma (2σ) for the same sample used for zircon (U-Th)/He dating. Considering the low helium closure temperature for apatite (~60-100 °C; Farley, 2002), these ages most likely represent the time of exhumation.

Methods

Drill core logging and petrography

Field relationships of the hypogene mineralization and alteration are primarily established via drill core logging. In this study, we have logged over 10,000 m of drill core along two orthogonal cross-sections (9-9` and C-C`; Fig. 2) that cross the entire ore zone and penetrate a depth up to 1000 m. Detailed drill core logging has enabled revealing a sequence of porphyries, chronological relationships of the veins, changes in vein types and abundance, transitions of alteration styles, and possible genetic relationships of the veins with individual porphyries. More than 1200 collected samples were augmented by a short-wave infrared absorption (SWIR) spectroscopic study to identify the distribution of fine-grained hydrous alteration minerals (see Appendix 1 for details of methods and results). About 500 sawed samples were visually examined using a binocular microscope, and over 300 polished thin sections were further studied under standard transmitted and reflected light microscopy to document the vein sequences and hydrothermal alteration assemblages.

Zircon U-Pb dating

Zircon grains were separated using conventional heavy liquid and magnetic separation techniques. Transparent and prismatic crystals were then hand-picked under a binocular microscope, and were mounted in epoxy resin and polished to expose the interiors of the grains. Transmitted- and reflected-light photomicrographs and cathodoluminescence (CL) images were used to characterize the internal textures of the grains and to guide U-Pb dating. LA-ICP-MS U-Pb dating was conducted at the State Key Laboratory of Geological Processes and Mineral Resources, China University of Geosciences, Wuhan. Detailed operating conditions for the laser ablation system and the ICP-MS instrument and data reduction follow those in Liu et al. (2010). Laser sampling was performed using a GeoLas 2005 instrument. An Agilent 7500a ICP-MS instrument was used to acquire ion-signal intensities. Zircon 91500 (1065 Ma) was used as an external standard for U-Pb dating, and was analyzed twice every 5 analyses. Preferred U-Th-Pb isotopic ratios used for 91500 are from

Wiedenbeck et al. (1995). The precision and accuracy of U-Th-Pb dating with this technique have been evaluated by comparison the ages of zircon standard GJ-1 analyzed in this study ($^{206}Pb/^{238}U$ ages of 594.3 ± 4.7 Ma to 600.6 ± 5.9 Ma; Appendix 2, Table A1) with that suggested by Jackson et al. (2004) ($^{206}Pb/^{238}U$ age of 599.8 ± 1.7 Ma). Uranium and Th contents were calibrated against the glass standard NIST SRM610 using Si for internal standardization. Off-line selection and integration of background and analytical signals, and time-drift corrections were performed by the in-house software ICPMSDataCal (Liu et al., 2010). Uncertainty in the preferred values for the external standard 91500 was propagated to the ultimate results of the samples. Concordia diagrams and weighted mean calculations were made using Isoplot/Ex (ver. 3.0; Ludwig, 2003).

Molybdenite Re-Os dating

Molybdenite-rich parts from various quartz veins were carefully cut to avoid mixing of different generations of molybdenite and then crushed to small pieces (~1-10 mm) using an agate pestle. Quartz-bearing molybdenite aggregates were hand-picked under a binocular microscope. We used HF to remove quartz from the mixed samples (Lawley and Selby, 2012) rather than traditional mechanical (crushing/sieving) separation protocols, because of the small grain-size (<0.2 mm) of the molybdenite. The quartz-bearing molybdenite aggregates were placed in a Savillex Teflon digestion vessel with 8 ml of 32N HF and left at room temperature for 24 hours (Lawley and Selby, 2012). This digestion process was repeated until most of the quartz has been digested. The HF was then removed by rinsing the molybdenite three times with MQ, and further rinsed by ethanol. After dried at 25 °C, the molybdenite was again handpicked under a binocular microscope and cleaned in an ultrasonic bath to reach a purity of better than 95 %.

Samples were analyzed at the Laboratory for Sulfide and Source Rock Geochronology and Geochemistry at Durham University, a member of the Durham Geochemistry Centre. Analytical procedures for rhenium (Re) and osmium (Os) contents and isotopic compositions of molybdenite mineral separates have been well

established and widely applied (Selby and Creaser, 2001; Markey et al., 2007; Selby et al., 2007; Porter and Selby, 2010; Lawley and Selby, 2012; Li et al., in press). The spike solution (^{185}Re + isotopically normal Os) used in this study was manufactured and calibrated (^{185}Re only, ± 0.15%, Os is gravimetrically determined, ± 0.14%) using the same protocol and standard solutions (Re only) outlined in Selby and Creaser (2001). This is also identical to the methodology outlined in Markey et al. (2007). In brief, a weighed aliquant of molybdenite mineral separate plus a spike solution (^{185}Re + isotopically normal Os) were loaded into a Carius tube with 11N HCl (1 ml) and 15.5N HNO_3 (3 ml), sealed, and digested at 220 °C for ~24 hr. Osmium was purified from the acid medium using solvent extraction ($CHCl_3$) at room temperature and microdistillation methods. The Re fraction was isolated by sodium hydroxide-acetone solvent extraction and standard anion column chromatography. The purified Re and Os were loaded onto coated Ni and Pt filaments, respectively, and their isotopic compositions were measured using Negative Thermal Ionization Mass Spectrometry (Creaser et al., 1991). The analyses were conducted on a Thermo Electron TRITON mass spectrometer, with Re and Os isotope compositions being measured using the static Faraday collection model. Rhenium and Os concentrations, and Re-Os molybdenite data uncertainties are presented at the 2σ absolute level, which are determined through the propagation of uncertainties related to Re and Os mass spectrometer measurements, blank determinations (which are insignificant given the abundance of Re and ^{187}Os in the molybdenite samples), spike and standard isotopic compositions, and calibration uncertainties of ^{185}Re and ^{187}Os (Heumann, 1988; Selby and Creaser, 2004; Markey et al., 2007). Because a mixed ^{185}Re and Os tracer solution is used, uncertainties in weights of sample and tracer solution do not affect the calculated age, and are not considered. However, sample and tracer solution weight uncertainties are considered in determining the uncertainty in the Re and ^{187}Os concentrations. During this study, Re and Os blanks were <2.5 and 0.1 pg, respectively, with the ^{187}Os/^{188}Os of the blank being 0.25 ± 0.02. An analysis of the NIST molybdenite reference material, RM8599, returned an age in agreement with its suggested value (27.656 ± 0.022 Ma; Markey et al., 2007) and those determined at

Durham (27.65 ± 0.11 Ma; Table 3) (Porter and Selby, 2010; Lawley and Selby, 2012; Li et al., in press).

Emplacement History of the Yulong Porphyry Stock

Previous studies have recognized multiple stage of porphyry intrusions at Yulong. For example, early drill core logging has revealed an intrusive contact between the MGP and a granite porphyry (Ma, 1990; Zhang et al., 1997). Tang et al. (1995) noted that the MGP is cut by a quartz albite porphyry (QAP), which is several meters wide and more than 100 m long in a southwestern outcrop of the Yulong composite stock. The relative shallow depth of early drill cores and extensive supergene alteration in the upper zone of the deposit, however, made it difficult to characterize the temporal and spatial relationships of the porphyry intrusions. In view of crosscutting relationships and lithologic and textural results revealed by detailed drill core logging in this study (Fig. 4), the Yulong composite stock consists of three successive porphyry intrusions, with the volumetrically most important MGP being the earliest intrusion that was followed by K-feldspar granite porphyry (KGP) and then the QAP (Fig. 2). All the three porphyries have similar phenocrysts consisting of variable size and amount of K-feldspar, plagioclase, quartz, and biotite, with minor hornblende, which are dispersed in an aplitic groundmass dominated by quartz, K-feldspar, plagioclase, and/or biotite (Table 1).

The MGP hosts the majority of Cu and Mo mineralization of the deposit (Fig. 2). Recent open-pit mining has revealed a late-stage porphyry dike (lithologically similar to the MGP) intruding the main MGP in the northern part of the Yulong stock, both hosting abundant quartz ± sulfides veins. The presence of vein quartz xenoliths in the main MGP in drill core (Fig. 6E) also indicates an earlier hydrothermal event before the MGP. Therefore, the voluminous MGP is likely to have formed by at least two petrologically similar phases. However, no petrographic criteria was available to distinguish these potential multi-phases during our drill core logging.

The KGP occurs as <50-m-wide dikes intruding the MGP (Fig. 2, 5). Contacts

between the KGP and quartz vein-bearing MGP or hornfels are sharp (Fig. 4A), and unidirectional quartz textures (USTs) are occasionally developed in the KGP close to the contact zone with the MGP (Fig. 4C). The KGP can also be easily distinguished from the MGP in terms of abundance and grain sizes of phenocrysts, even when they are overprinted by intense supergene kaolinite leaching.

The latest QAP dikes, ranging in thickness from <0.5 to 25 m, typically truncate quartz veins hosted in the MGP or KGP (Fig. 4B, D). Angular to sub-rounded MGP and vein quartz xenoliths are frequently contained in the QAP. The unaltered QAP is darker than the other two porphyries owing to the lower proportion of phenocrysts and the presence of abundant magmatic biotite in the groundmass. Most of QAP dikes have been subjected to intense sericitic alteration with only the quartz phenocrysts and/or vein quartz xenoliths survived. Quartz veins rarely occur in the QAP, which is another feature distinct from the MGP and KGP (Fig. 5B).

Veins, Hydrothermal Alteration, and Sulfide Mineralization

Vein formation, hydrothermal alteration and Cu-Mo mineralization are grouped into early, transitional and late stages with respect to the intrusive history and change of mineralization/alteration styles (Table 2). Nomenclature of vein assemblages at Yulong is from Gustafson and Hunt (1975), Gustafson and Quiroga (1995), and Sillitoe (2010). Based on crosscutting relationships and spatial distribution of various veins, we have identified cyclical sequences of veining following the intrusion of the MGP (multistage?) and KGP, which include (1) M_E veins/UST_T, (2) $EB_{E/T}$ veins, (3) $A1_{E/T}$ veins, (4) $A2_E/B_T$ veins, and (5) $A3_{E/T}$ veins. These veins are largely associated with potassic alteration. Postdating the intrusion of QAP dikes are the youngest D_L veins closely associated with sericitic alteration. Except for the sericitic alteration, other two types of hydrolytic alteration, namely the intermediate argillic and advanced argillic alteration, have also been documented in the deposit. The characteristics, distribution and timing of different vein types, hydrothermal alteration, and mineralization are presented in Figures 4-10 and Appendix 1 and further discussed

below.

The early stage

The early stage veins, potassic alteration and associated mineralization predate the intrusion of KGP dikes. M_E and EB_E veins generally formed earlier than the barren $A1_E$ quartz veins (Fig. 6A, B). The granular quartz-dominated $A2_E$ veins are paragenetically earlier than the chalcopyrite ± pyrite-dominated $A3_E$ veins (Fig. 6E, G). $A2_E$ and $A3_E$ veins are the major Cu and Mo carriers of the early stage. Molybdenite predominantly occurs as disseminations in $A2_E$ veins, whereas chalcopyrite occurs in both $A3_E$ and $A2_E$ veins (Fig. 6D-G). The mutual crosscutting relationships between EB_E, $A1_E$ and $A2_E$ veins likely indicate multistage magmatic-hydrothermal pulses (Fig. 6B-D, F). Figure 8 illustrates the density distribution of all quartz-dominated vein types, namely M_E, $EB_{E/T}$, $A1_{E/T}$, $A2_E$, and B_T veins. The overall density roughly reflects the distribution of $A1_E$ veins (locally >30 vol.%) in the barren core and $A2_E$ veins (5-10 vol.%) in the mineralized zone in the MGP, as they are much more abundant than the other quartz-dominated vein types. The intense potassic alteration in the barren core (Fig. 9) consists of fine-grained quartz, K-feldspar and biotite with the porphyry texture being completely obliterated, and are characterized by texture-destructive replacement of the MGP with very low density of quartz veins (Fig. 7A) or high density fracture filling $A1_E$ veins with the MGP residues (Fig. 7B), both cases indicating the former presence of voluminous hydrothermal fluids in the barren core. In contrast, $A2_E$ and $A3_E$ veins are mainly localized in zones of strong to weak potassic alteration adjacent to the barren core, as best illustrated by the Cu and Mo mineralization above ~4300 m a.s.l. (Fig. 8).

The transitional stage

The transitional stage postdates the KGP, but predates the intrusion of QAP dikes. EB_T veins are rarely observed in the KGP, and unexceptionally cut by the barren $A1_T$ quartz veins (<10 vol.%; Fig. 4A, 5). Both UST_T and $A1_T$ veins in KGP dikes are truncated by B_T veins (<5 vol.%; Figs. 4C, 8). No mutual crosscutting relationship of B_T veins was observed in this study. B_T veins typically have banded textures without

visible alteration halos or occasionally associated with thin sericitic halos (Fig. 6C, I). The latter may be the result of overprinting by D_L veins. Molybdenite in B_T veins typically occurs on margins of these veins, and is intergrown with anhedral, granular quartz ± K-feldspar ± anhydrite, which are normally overgrown by euhedral, free-standing quartz pointing into central voids of these veins with various chalcopyrite ± pyrite fillings. These characteristics are comparable with "B" type veins developed in many other PCDs (Gustafson and Hunt, 1975; Sillitoe, 2010), and make it easy to distinguish them from $A2_E$ veins. B_T veins are actually mineralized equivalent to $A2_E$ veins, but appear to contain more abundant molybdenite. The chalcopyrite ± pyrite-dominated $A3_T$ veins hosted by the KGP show no difference with $A3_E$ veins (Fig. 6H). The Mo grade can be as high as 0.1 wt% in the KGP due to the common presence of B_T veins (Fig. 5). However, the Cu grade is generally <0.5 wt%, which is controlled by chalcopyrite in B_T and $A3_T$ veins. Most of B_T veins are closely associated with the deep-seated, Mo-rich zone under ~4300 m a.s.l. (Fig. 8).

The late stage

The late stage postdates the emplacement of QAP dikes, and is characterized by pyrite ± quartz veins with well-developed sericitic alteration halos (D_L veins), as well as zones of pervasive sericitic alteration overprinting the precursory potassic alteration. D_L veins occur in all porphyries, and either cut or refill all the other vein types (Figs. 4B, 6I). Quartz-dominated veins rarely occur in QAP dikes, which, in many cases, have been intensely altered to form sericitic assemblages with the intensity of the alteration decreasing toward the surrounding MGP or KGP (Fig. 5B). A large amount of pyrite and minor chalcopyrite, tennantite, enargite, sphalerite, and galena are observed in the altered QAP dikes; this mineral assemblage is consistent with the unexceptionally low Cu (<0.3 wt%) and Mo (<0.01 wt%) grades but high S contents in QAP dikes (e.g., Fig. 5B). An 8-m-thick QAP dike was observed intruding the skarn ore (Fig. 10). The sharp contrast of Cu and S grades between the skarn ore and the QAP dike indicates that the Cu skarn mineralization formed earlier before the intrusion of QAP dikes.

Zonation and overprinting of hydrothermal alteration

The hydrothermal alteration zonation typical of PCDs has been documented at Yulong (Du, 1985; Tang et al. 1995), and is illustrated in the two cross-sections mainly based on the drill core logging results (Fig. 9). The potassic and propylitic alteration form several concentric alteration zones shifting from the intense potassic alteration in the core of the Yulong stock to the propylitic alteration in the distal hornfels. Potassic alteration assemblages are largely expressed by K-feldspar, biotite, quartz, with minor amount of magnetite, actinolite, epidote, albite, carbonate, and anhydrite. The decreasing intensity of potassic alteration is mainly manifested by the increasing degree of porphyry texture preservation, and the strong to moderate potassic alteration tends to contain more hydrothermal biotite but less hydrothermal K-feldspar ± quartz than intense potassic alteration assemblages (Fig. 7). The propylitic alteration consists of epidote, chlorite, albite, calcite, and pyrite which occur as fine-grained aggregates or veinlets in the weakly metasomatized hornfels (Du, 1985). The most pervasive veining and mineralization in the early stage suggest that the potassic and propylitic alteration zonation pattern in the MGP and hornfels were produced during this stage, though the transitional stage veining is also associated with strong to moderate potassic alteration assemblages in the KGP.

The hydrolytic alteration is ubiquitous throughout the deposit, and normally overprints the precursory potassic altered rocks (Du, 1985; this study). Integrated SWIR spectral analysis (App. 1) and petrographic observations on selected samples and thin sections suggest that the hydrolytic alteration at Yulong can be grouped into three types, i.e., sericitic, intermediate argillic and advanced argillic alteration (cf. Meyer and Hemley, 1967; Seedorff et al., 2005), which are largely represented by muscovite, montmorillonite, and dickite (or nacrite), respectively, as best illustrated in Figures A1-2. The sericitic alteration is dominated by quartz-pyrite-muscovite ± illite ± kaolinite (?) assemblages, and has resulted from complete or partial destruction of the precursory potassic assemblages (Fig. 6I). Sericitic assemblages are considered to be produced in the late stage, because they are closely associated with QAP dikes

(Figs. 9, A1-2). The intermediate argillic alteration is composed of illite + montmorillonite ± kaolinite that variably replace plagioclase phenocrysts but does not affect K-feldspar and biotite (Fig. 6B, C). Intermediate argillic assemblages appear to be unrelated to any vein type, and are not accompanied by sulfides. They commonly overprint the moderate potassic alteration zone, but are less common in the intensely potassic altered zone. This contrast is likely due to the lack of plagioclase in the intensely potassic altered zone, where plagioclase phenocrysts had been totally replaced by K-feldspar in earlier stages. Intermediate argillic assemblages typically formed at relatively low temperature (below to ~200 °C; Seedorff et al., 2005) and are developed in all porphyry intrusions at Yulong (Fig. 4B, D), indicating they are products of the late stage. However, the lack of spatial relationship with QAP dikes (Figs. A1-2) suggests that the intermediate argillic alteration might also have formed during retrograde processes of the early and transtional stages. The advanced argillic alteration is represented by the rare dickite-kaolinite assemblages. As advanced argillic assemblages are found both in the MGP and KGP, and mainly restrict to deep parts of the deposit (<4300 m a.s.l.), they are most likely part of the late stage events.

Distribution of supergene kaolinite ± montmorillonite (?) alteration zone is also shown for reference (Fig. 9). Kaolinite is normally the only type of hydrous mineral in the shallow strong supergene kaolinite leached zone (Figs. A1-2).

Cu-Mo mineralization intensity of the three stages

Based on the distribution, sulfide contents and vein density, as well as the spatial distribution of Cu and Mo grades revealed from the two studied cross-sections, it is estimated that at least 80 % of Cu and Mo were deposited during the early stage, with the remainder being results of the transitional stage. No economic Cu and Mo mineralization has been introduced during the late stage. During the transitional stage, more Mo was introduced relative to Cu, but the reverse applies to the early stage. This view is supported by two observations: (1) the KGP has relatively low Cu grade, and (2) the deep Mo-rich but Cu-poor zone (<4300 m a.s.l.) is dominated by B_T veins. Nevertheless, the amount of chalcopyrite that precipitated as sulfide-dominated veins

during the transitional stage in the upper part of the MGP (>4300 m a.s.l.) is unclear.

Zircon U-Pb Ages of Porphyry intrusions

Three samples of the MPG (sample 1007-988), KGP (sample 0908-308) and QAP (sample 1303-280) were collected from drill cores for zircon separation and U-Pb dating (Fig. 2). Zircon crystals from all three samples exhibit similar characteristics. They are transparent and colorless, ranging in size from 50 to 300 μm with an elongation ratio of 1-3:1. The CL images show that the majority of grains have planar or oscillatory concentric zoning (Fig. 11), which is indicative of a magmatic origin (Corfu et al., 2003). All the analyses were conducted on the rim of individual zircon grains. The LA-ICP-MS zircon U-Pb data are illustrated on concordia diagrams (Fig. 11) and tabulated in Appendix 2 (Table A1).

Eighteen of 20 analyses from the MGP (sample 1007-988) are concordant or marginally concordant, with $^{206}Pb/^{238}U$ ages ranging from 42.8 ± 0.5 to 41.2 ± 0.5 Ma. One analysis (1007-988-9) is slightly discordant. This discordant grain, however, has a $^{206}Pb/^{238}U$ age (41.6 ± 0.5 Ma) indistinguishable from the concordant ones. The nineteen analyses have a weighted mean $^{206}U/^{238}Pb$ age of 42.0 ± 0.3 Ma (2σ, MSWD = 0.65; Fig. 11A), which is interpreted as the best estimate of the crystallization age of the MGP. The remaining grain with a much older $^{206}U/^{238}Pb$ age of 241.3 ± 3.3 Ma (Table A1) is considered to be an inherited zircon.

Twenty U-Pb analyses were performed on the KGP (sample 0908-308), 18 of which yield a weighted mean $^{206}U/^{238}Pb$ age of 41.2 ± 0.3 Ma (2σ, MSWD = 1.3; Fig. 11B). Of these, twelve spot analyses are concordant, and six are discordant. The $^{206}Pb/^{238}U$ ages of the discordant grains are indistinguishable from the concordant ones, indicating that the discordance is most likely caused by uncertainties in the ^{207}Pb measurement. The two dismissed grains have younger $^{206}U/^{238}Pb$ ages of 39.0 ± 0.4 Ma and 36.8 ± 0.4 Ma that could be due to minor lead loss.

Twenty analyses were carried out on 20 grains of the QAP (sample 1303-280). Fourteen analyses are concordant and give $^{206}Pb/^{238}U$ ages from 39.5 ± 0.5 to 40.6 ±

0.5 Ma, with a weighted mean of 40.2 ± 0.3 Ma (MSWD = 0.35; Fig. 11C). This age is interpreted to be the best estimation of the emplacement age of QAP dikes. The remaining six concordant or marginally concordant spots yield slightly older $^{206}U/^{238}Pb$ ages from 42.1 ± 0.5 to 43.2 ± 0.6 Ma, which could be the age of xenocrysts from early porphyry intrusions considering the common occurrence of MGP xenoliths in QAP dikes.

Collectively, the $^{206}U/^{238}Pb$ ages appear to be consistent with successive magmatic intrusions of the MGP, KGP, and QAP as deduced from intrusive relationships. However, estimating both the timescale of magmatism and mineralization based on these data is challenging considering the relatively large analytical uncertainties intrinsic to the LA-ICPMS technique (Table A1; Fig. 11). Further studies using high-precision U-Pb CA-IDTIMS analysis would provide tight constraints on the time interval of each magmatic intrusion (cf. Chiaradia et al., 2013; Schaltegger et al., 2015).

Re-Os Ages of Molybdenite-bearing Quartz Veins

Fourteen molybdenite-bearing quartz veins covering the entire vertical extent of the deposit were collected for molybdenite separation and Re-Os dating (Fig. 2), including six early stage $A2_E$ veins and eight transitional stage B_T veins (Fig. 12). Four $A2_E$ veins were taken from the drill hole ZK1303 over a vertical interval of ~400 m exhibiting distinct ore grades. The other two $A2_E$ veins were taken from drill holes ZK0705 (sample 0705-155) and ZK0905 (sample 0905-159). Sample 0905-159 is a quartz-sulfides vein with molybdenite occurring as fracture infillings (Fig. 12I). Eight B_T vein samples were selected from various host rocks (i.e., MGP, KGP and hornfels) over a vertical extent of 750 m. Most of the samples have variably suffered from the intermediate argillic, sericitic or supergene kaolinite alteration after vein formation (Table 3).

The Re-Os abundances and model age dates, including the absolute uncertainties at 2σ level are reported in Table 3. The $A2_E$ vein from sample 1303-390 has the oldest

Re-Os model age of 42.28 ± 0.17 Ma. Four other $A2_E$ vein samples (0705-155, 1303-484, 1303-114, and 1303-256) have model ages that are indistinguishable within analytical uncertainties (41.77 ± 0.17 Ma, 41.75 ± 0.17 Ma, 41.75 ± 0.17 Ma, and 41.46 ± 0.17 Ma, respectively). Molybdenite in the $A2_E$ vein from sample 0905-159, occurring as fracturing infillings, yields a model age of 40.95 ± 0.17 Ma. This Re-Os date is in agreement with the age of most of B_T veins (see below). This age consistency indicates that the fracture-filling molybdenite formed during the transitional stage. Six B_T veins hosted by the MGP and KGP yield perfectly consistent dates of 40.92 ± 0.17 to 40.98 ± 0.17 Ma, whereas the other two samples (1303-405 and 0505-455) have significantly younger ages of 39.56 ± 0.17 Ma and 37.15 ± 0.15 Ma, respectively. Molybdenites in the $A2_E$ veins have Re concentrations ranging from 127 to 526 ppm, whereas those from the B_T veins tend to have much lower values (18-277 ppm). However, no clear relationship between Re concentration and age is observed.

Numerous studies have shown that molybdenite Re-Os dating is a remarkably robust geochronometer, even when the mineral has been subjected to post-ore thermal processes (e.g., Stein et al., 1998; Selby and Creaser, 2001; Selby et al., 2002; Stein, 2006; Stein, 2014; Spencer et al., 2015). However, dating results may be significantly affected by Re and Os decoupling in the mineral (Stein et al., 1998, 2003; Kosler et al., 2003; Selby et al., 2003, 2004; Selby and Creaser, 2004). The degree of decoupling between Re and ^{187}Os appears to be related to the crystal grain size and age of molybdenite, with young and fine-grained molybdenite being least affected (Stein et al., 2003; Selby et al., 2003, 2004; Selby and Creaser, 2004). Molybdenite samples in this study are less than 2 mm in size (Table 3), indicating that Re and ^{187}Os decoupling can be overcome by analyzing 10 mg samples of the molybdenite mineral separates (Selby and Creaser, 2004; Lawley and Selby, 2012). Therefore, molybdenite Re-Os ages presented here are considered reliable and can be interpreted as the best estimates for mineralization age of the Yulong porphyry Cu-Mo deposit.

Discussion

Evolution and lifetime of the Yulong porphyry Cu-Mo deposit

Porphyry Cu-(Mo-Au) systems are typically developed in the upper 4 km of the crust, with their centrally located stocks being connected downward to parental magma chambers at depths of perhaps 5-15 km (cf. Sillitoe, 2010). The Al-in-hornblende barometer of the MGP at Yulong suggests that hornblende phenocrysts formed at 2-3 kbar, equivalent to a depth of 6-9 km (Ma, 1990). This estimation suggests that the parental magma chamber responsible for the Yulong deposit shared a common depth range to many other large porphyry Cu systems. Voluminous fluids exsolved from the magma chamber and migrated upward primarily in three field-distinguishable stages (the early, transitional and late stages), which followed the intrusion of the MGP, KGP and QAP, respectively. Each of the three stages has resulted in variable hydrothermal alteration, vein formation and/or Cu-Mo mineralization (Fig. 13).

The barren but intensely potassic altered and/or highly veined core of the deposit, formed immediately after the intrusion of the MGP, is interpreted to have acted as the focus of upwelling magmatic-hydrothermal fluids during the early stage. These fluids flowed upward and outward to cause the gradually weakening potassic alteration to distal propylitic alteration, and the lower density of quartz vein associated with Cu-Mo mineralization surrounding the central fluid plume. This inferred process is recorded by the upward/outward distribution and sequential formation of M_E, EB_E, $A1_E$, $A2_E$, and $A3_E$ veins. Several lines of geologic evidence suggest this process happened cyclically in at least two episodes: (1) the crosscutting relationship of two generations of the MGP that both contain quartz veins; (2) the presence of xenoliths of quartz ± sulfides veins in the MGP (Fig. 6E); (3) two distinct styles of intense potassic alteration in the barren core (Fig. 7A, B); (4) reverse crosscutting of EB_E veins by $A1_E$ and $A2_E$ veins (Fig. 6C, D), and (5) offsetting relationships of several generations of $A2_E$ veins (Fig. 6E, F). The molybdenite Re-Os age of the oldest $A2_E$ vein is resolvable within uncertainty from the other four $A2_E$ veins with a nominal

time gap of 0.51 ± 0.24 m.y. (1σ), which further confirms the cyclical formation of $A2_E$ veins by discrete ore-forming fluid pulses. The Re-Os ages of the five $A2_E$ veins combined indicate that the early stage mineralization occurred over an extended period of 0.82 ± 0.24 m.y. (1σ). Previous isotopic dating and thermodynamic modeling have demonstrated that the emplacement of an individual intrusion and subsequent focusing of large fluid fluxes associated with PCDs typically lasts for a duration of 0.01 to 0.1 m.y. (von Quadt et al., 2011; Buret et al., 2016; Spencer et al., 2016), and the maximum lifespan of an individual magmatic-hydrothermal pulse could be even shorter (Cathles et al., 1997; Driesner and Geiger, 2007). Therefore, we argue that more discrete mineralization events (cyclical pulses) during the early stage, with or without precursory porphyry intrusions, could potentially be identified by improving analytical precision and dating more $A2_E$ veins.

Following the intrusion of KGP dikes, magmatic-hydrothermal fluids of the transitional stage flowed upward through similar deep paths to the early stage, considering the distribution of B_T veins overlaps the deep parts of the early stage mineralization and alteration (Fig. 8). The formation of a full vein sequence (UST_T, EB_T, $A1_T$, B_T, and $A3_T$ veins) associated with strong to moderate potassic alteration in the KGP is comparable to the early stage, but the much lower vein density and weaker mineralization of this stage suggest a significantly smaller volume of ore-forming fluids. All the molybdenite Re-Os ages of B_T veins from various host rocks are consistently younger than the five $A2_E$ veins, strongly supporting the field-based chronology of porphyry intrusion, vein formation and Cu-Mo mineralization. Given that $A2_E$ veins were emplaced before the intrusion of the KGP, and that B_T veins are commonly hosted by the KGP, the age of KGP dikes can be constrained at between 41.46 ± 0.17 and 40.96 ± 0.16 Ma. Seven out of the nine dated B_T veins, spanning a vertical extent of >750 m in different parts of the deposit (Fig. 2), have extremely consistent Re-Os ages of 40.98 ± 0.23 to 40.92 ± 0.17 Ma. We thus interpret the bulk Mo ± Cu ores of the transitional stage to have formed rapidly. In contrast, the other two significantly younger B_T veins (39.56 ± 0.17 and 37.15 ± 0.15 Ma) represent two successive individual magmatic-hydrothermal mineralization events. They likely

formed later than the intrusion of the QAP, at least for the younger molybdenite, which possesses a Re-Os age (37.15 ± 0.19 Ma including the uncertainty of the ^{187}Re decay constant) younger than the zircon U-Pb age of the QAP (40 ± 2 Ma with external uncertainty of ~4%; Li et al., 2015). We suggest that the two younger events, therefore, are unlikely to have significantly contributed to the bulk ore formation, and probably reflect magmatic-hydrothermal resurgence in the magma chamber.

The intrusion of QAP dikes marks the waning stage of ore-forming fluid input. D_L veins and the closely associated sericitic alteration overprinted and completely or partially destroyed the earlier potassic alteration assemblages, with significant sulfidation but little or no addition of Cu or Mo (Fig. 5B). The widespread intermediate argillic alteration can form as a low-temperature equivalent to the sericitic alteration during the late stage, and is also likely to be produced from the cooled ore-forming fluids of the early and transitional stages after ore precipitation. The uncommon advanced argillic alteration in deep barren parts of the deposit could have formed by a low-temperature and acid fluid during the late stage (Seedorff et al. 2005).

Neither previous U-Pb, Re-Os, and (U-Th)/He dating of different minerals nor the present zircon U-Pb dating of different porphyries can precisely determine the longevity of Cu-Mo mineralization at Yulong. The reasons are: (1) *in-situ* zircon dating techniques (LA-ICP-MS, SIMS, and SHRIMP) do not provide the necessary precision to resolve the timescales of Cu-Mo precipitation (von Quadt et al., 2011; Chiaradia et al., 2013; Buret et al., 2016), (2) existing ID-ICPMS Re-Os data of molybdenite-quartz veins from Yulong deposit have low analytical precision (lower than 1.4 %) and the relative chronology of the dated veins were not established in the field or petrologically (Hou et al., 2006; Tang et al., 2009), and (3) (U-Th)/He dating on zircon and apatite only provides cooling history of a system (Li et al., 2012). In this study, the dated $A2_E$ and B_T veins were collected from the two field-separated stages, and span the entire vertical extent of the deposit (Fig. 2). In addition, the new molybdenite Re-Os ages obtained by ID-NTIMS have much higher precision (~0.4 %) than all previous studies, making it possible to place tight constraints on the timing

and duration of the Cu-Mo mineralization at Yulong.

In summary, the Yulong porphyry Cu-Mo deposit was produced in more than five magmatic-hydrothermal pulses spanning a time period of 5.13 ± 0.23 m.y. (1σ), although the bulk Cu-Mo mineralization formed in a much shorter interval of 1.36 ± 0.24 m.y. (1σ) from 42.28 ± 0.17 to 40.92 ± 0.17 Ma (Fig. 13). Protracted mineralization histories (1.5-4 m.y.) have also been reported in some world-class PCDs elsewhere by integrating zircon U-Pb and other geochronometers (Sillitoe and Mortensen, 2010 and reference therein), but only recently by Re-Os molybdenite dating alone (Deckart et al., 2012; Stein, 2014; Spencer et al., 2015; Li et al., in press). Our results demonstrate that, based on detailed field relationships and extensive sampling, high precision Re-Os molybdenite dating can indeed provide significant insights into the timing, duration, and evolution of magmatic-hydrothermal mineralization responsible for PCD formation.

Formation of a giant porphyry Cu deposit

The key factors controlling the generation of a giant PCD is an outstanding question in economic geology (Cooke et al., 2005; Wilkinson, 2013; Richards, 2013). Long-lived hydrothermal systems versus short-lived hydrothermal systems in forming a giant PCD has long been a matter of debate (e.g., Cathles et al., 1997; Sillitoe and Mortensen, 2010; Chiaradia et al., 2013; Chiaradia and Caricchi, 2017). The Yulong deposit contains proven reserves of ~6.5 Mt Cu. Considering that the shallow part of the ore zone must have been eroded as indicated by the widespread gossans and supergene enrichment zones of huge thickness (Deng et al., 2017), it is likely that the deposit originally contained over 10 Mt Cu, and thus can be counted as a giant to supergiant PCD (giant: 3.162 to 10 Mt Cu; supergiant: 10 to 31.62 Mt Cu; as defined in Clark, 1993). The geologic and geochronologic constraints at the long-lived Yulong deposit, when combined with high-precision geochronological results from other PCDs, make it possible to explore the role of lifetime of magmatic-hydrothermal system in the formation of a giant or supergiant PCD.

The overall longevity of the Yulong deposit (~5 m.y.) implies a preexisting

long-lived parental magma chamber, but the bulk Cu-Mo mineralization formed in a much shorter period of 1.36 ± 0.24 m.y. (Fig. 14). In fact, most of the Cu at Yulong (>80 %) was deposited in a more restricted timespan of 0.82 ± 0.24 m.y. in several individual magmatic-hydrothermal pulses during the early stage. Recent detailed Re-Os dating of molybdenite from veins representing different mineralization stages at Los Pelambres-El Pachón, Rio Blanco-Los Bronces, and El Teniente also suggest prolonged durations of Cu-Mo mineralization in these systems (~1.85 m.y., ~2.2 m.y., and ~1.9 m.y., respectively; Stein, 2014; Deckart et al., 2014; Spencer et al., 2015). These PCDs represent the world's supergiant or the largest PCDs (Los Pelambres-El Pachón, 26.88 Mt Cu; Rio Blanco-Los Bronces, 56.73 Mt Cu; El Teniente, 94.35 Mt Cu; Cooke et al., 2005) that are characterized by overprinting of mineralized envelopes from several isolated, fertile intrusion centers (Vry et al., 2010; Deckart et al., 2012). Spencer et al. (2015) argued that the isolated intrusion centers acted as effective, short-lived (<0.1 m.y.) conduits for pulses of Mo- and Cu-bearing hydrothermal fluids during the lifetime of El Teniente. Extensive Re-Os dating results at El Teniente indicate that the majority of Cu could have formed in ~0.4 m.y. from 5.0 to 4.6 Ma (Maksaev et al., 2004; Cannell et al., 2005; Spencer et al., 2015). This case may also be applicable to Los Pelambres-El Pachón and Rio Blanco-Los Bronces, i.e., the majority of Cu formed in a much more restricted duration, because of the significant heterogeneous introduction of Cu in different stages (Atkinson et al., 1996; Deckart et al., 2012). Short mineralization duration has actually been demonstrated in several PCDs (Fig. 14; Bingham, von Quadt et al., 2011; Alumbrera, Buret et al., 2016; Qulong, Li et al., in press). For examples, high precision CA-ID-TIMS ages of the youngest zircons in pre-ore and post-ore intrusions overlap within a time interval of 0.32 m.y. at Bingham Canyon (28.46 Mt Cu) and 0.029 m.y. at Bajo de la Alumbrera (2.17 Mt Cu), which are interpreted as the maximum duration of several pulses of porphyry emplacement and associated ore formation (von Quadt et al., 2011; Buret et al., 2016). Nevertheless, a longer lifetime of the subjacent magma reservoir (>1-2 m.y.) in these two systems is indicated by formation ages of all the zircon dated.

Taken together, the available geochronological and geological data suggest that

multiple magmatic-hydrothermal pulses in tens to hundreds of thousands of years or even shorter is sufficient enough to form a giant to supergiant PCD, though a lifetime of more than one to a few million years of the parental magma chamber seems to be necessary as documented in a recent stochastic modeling study (Chiaradia and Caricchi, 2017). Therefore, the metal concentration, volume and focusing efficiency of ore-forming fluids (Audétat et al., 2008), cyclically deriving from a long-lived parental magma chamber, could have played critically important roles in forming a giant PCD regardless of a short- or long-lived magmatic-hydrothermal system.

Conclusions

The spatial and temporal relationships of porphyry intrusions, various vein types, hydrothermal alteration assemblages and Cu-Mo mineralization at Yulong are established based on detailed drill core logging and petrographic study. After the successive intrusion of the MGP and KGP, several cyclical sequences of veining developed during the early and transitional stages. These are, from early to late, (1) M_E vein/UST_T, (2) $EB_{E/T}$ veins, (3) $A1_{E/T}$ veins, (4) $A2_E/B_T$ veins, and (5) $A3_{E/T}$ veins that are mainly associated with potassic alteration. Most Cu and Mo (>80 %, probably more Cu) of the deposit are associated with the early stage $A2_E$ and $A3_E$ veins, with the remaining significant amount of Mo (~20 %) hosted by the transitional stage Mo-rich B_T veins. The potassic and propylitic alteration in the deposit, which are mainly developed during the early stage, form several concentric alteration zones shifting from the intense potassic alteration in the barren core to the propylitic alteration in the distal hornfels. Some intermediate argillic alteration is inferred to be developed during the early and transitional stages when the multiple pulses of ore-forming fluids cool to ~200 °C. The intrusion of QAP dikes is followed by the late stage D_L veins and sericitic alteration with no economic Cu-Mo mineralization, which marks the waning of ore-forming fluid input. The low-temperature intermediate argillic and advanced argillic alteration also formed during the late stage.

The robust molybdenite Re-Os geochronology provides improved constraints on

the ore-forming process at Yulong. Results suggest that molybdenite and chalcopyrite deposition was episodic over a prolonged history lasting over 5.13 ± 0.23 m.y., but the bulk Cu-Mo ore formed in a much shorter time interval of 1.36 ± 0.24 m.y. As most Cu at the Yulong deposit could have formed in a more restricted timespan of 0.82 ± 0.24 m.y., we conclude that the metal concentration, volume and focusing efficiency of ore-forming fluids could have played more important roles in forming a giant to supergiant PCD like Yulong rather than a long-lived magmatic-hydrothermal system.

Acknowledgments

This research was jointly funded by the National Natural Science Foundation of China (grant No. 41325007) and the GPMR State Key Laboratory (MSFGPMR03). DS acknowledges the Total endowment fund. Shen-Tai Liu and Yong-gang Liu are thanked for providing access to the mine site and drill core. The authors also wish to thank Shi-Da Lu and De-Rong Ma for their help in molybdenite separation. Yang Li provided useful comments on an early version of this paper. Constructive reviews by Prof. Zengqian Hou and editorial suggestions by Prof. Larry D Meinert and Dr. Massimo Chiaradia are gratefully appreciated. This is the second contribution from CODME (Center for Ore Deposits and Mineral Exploration).

REFERENCES

Atkinson, J. W. W., Souviron, A., Vehrs, T. I., and Faunes, A., 1996, Geology and mineral zoning of the Los Pelambres porphyry copper deposit, Chile: Society of Economic Geologists Special Publication 5, p. 131-156.

Audétat, A., Pettke, T., Heinrich, C. A., and Bodnar, R. J., 2008, Special paper: the composition of magmatic-hydrothermal fluids in barren and mineralized intrusions: Economic Geology, v. 103, p. 877-908.

Braxton, D. P., Cooke, D. R., Dunlap, J., Norman, M., Reiners, P., Stein, H., and Waters, P., 2012, From crucible to graben in 2.3 Ma: A high-resolution geochronological study of porphyry life cycles, Boyongan-Bayugo copper-gold deposits, Philippines: Geology, v. 40, p. 471-474.

Buret, Y., von Quadt, A., Heinrich, C., Selby, D., Wälle, M., and Peytcheva, I., 2016, From a long-lived upper-crustal magma chamber to rapid porphyry copper emplacement: Reading the geochemistry of zircon crystals at Bajo de la Alumbrera (NW Argentina): Earth and Planetary Science Letters, v. 450, p. 120-131.

Cannell, J., Cooke, D. R., Walshe, J. L., and Stein, H., 2005, Geology, mineralization, alteration, and structural evolution of the El Teniente porphyry Cu-Mo deposit: Economic Geology, v. 100, p. 979-1003.

Cathles, L. M., Erendi, A., and Barrie, T., 1997, How long can a hydrothermal system be sustained by a single intrusive event? Economic Geology, v. 92, p. 766-771.

Chiaradia, M., and Caricchi, L., 2017, Stochastic modelling of deep magmatic controls on porphyry copper deposit endowment: Scientific Reports, v. 7.

Chiaradia, M., Schaltegger, U., Spikings, R., Wotzlaw, J., and Ovtcharova, M., 2013, How accurately can we date the duration of magmatic-hydrothermal events in porphyry systems?—an invited paper: Economic Geology, v. 108, p. 565-584.

Clark, A. H., 1993, Are outsize porphyry copper deposits either anatomically or environmentally distinctive: Society of Economic Geologists Special Publication, v. 2, p. 213-283.

Cooke, D. R., Hollings, P., and Walshe, J. L., 2005, Giant porphyry deposits: characteristics, distribution, and tectonic controls: Economic Geology, v. 100, p. 801-818.

Corfu, F., Hanchar, J. M., Hoskin, P. W., and Kinny, P., 2003, Atlas of zircon textures: Reviews in Mineralogy and Geochemistry, v. 53, p. 469-500.

Creaser, R. A., Papanastassiou, D. A., and Wasserburg, G. J., 1991, Negative thermal ion mass spectrometry of osmium, rhenium and iridium: Geochimica et Cosmochimica Acta, v. 55, p. 397-401.

Deckart, K., Clark, A. H., Cuadra, P., and Fanning, M., 2012, Refinement of the time-space evolution of the giant Mio-Pliocene Río Blanco-Los Bronces porphyry Cu-Mo cluster, Central Chile: new U-Pb (SHRIMP II) and Re-Os geochronology and $^{40}Ar/^{39}Ar$ thermochronology data: Mineralium Deposita, v. 48, p. 57-79.

Deckart, K., Silva, W., Spröhnle, C., and Vela, I., 2014, Timing and duration of hydrothermal activity at the Los Bronces porphyry cluster: an update: Mineralium Deposita, v. 49, p. 535-546.

Deng, X. D., Li, J. W., Shuster D. L., 2017. Late Mio-Pliocene chemical weathering of the Yulong porphyry Cu deposit in the eastern Tibetan Plateaau constrained by goethite (U-Th)/He dating: Implications for Asian summer monsoon. Earth and Planetary Science Letters, https://doi.org/10.1016/j.epsl.2017.04.043.

Driesner, T., and Geiger, S., 2007, Numerical simulation of multiphase fluid flow in hydrothermal systems: Reviews in Mineralogy and Geochemistry, v. 65, p. 187-212.

Du, X. F., 1985, The character of the alteration and mineralization zones of the porphyry copper-molybdenite deposit in eastern Tibet and its comparison with the J.D. Lowell model: Contribution to the Geology of the Qinghai-Xizang (Tibet) Plateau, v. 17, p. 369-382.

Farley, K. A., 2002, (U-Th)/He dating: techniques, calibrations, and applications: Reviews in Mineralogy and Geochemistry, v. 47, p. 819-844.

Guo, L. G., Liu, Y. P., Xu, W., Zhang, X. C., Qin, K. Z., Li, T. S., and Shi, Y. R., 2006, Constraints to the mineralization age of the Yulong porphyry copper deposit from SHRIMP U-Pb zircon data in Tibet: Acta Petrologica Sinica, v. 22, p. 1009-1016.

Gustafson, L. B., and Hunt, J. P., 1975, The porphyry copper deposit at El Salvador, Chile: Economic Geology, v. 70, p. 857-912.

Gustafson, L. B., and Quiroga, J., 1995, Patterns of mineralization and alteration below the porphyry copper orebody at El Salvador, Chile: Economic Geology, v. 90, p. 2-16.

Harris, A. C., Dunlap, W. J., Reiners, P. W., Allen, C. M., Cooke, D. R., White, N. C., Campbell, I. H., and Golding, S. D., 2008, Multimillion year thermal history of a porphyry copper deposit: application

of U-Pb, $^{40}Ar/^{39}Ar$ and (U-Th)/He chronometers, Bajo de la Alumbrera copper-gold deposit, Argentina: Mineralium Deposita, v. 43, p. 295-314.

Heumann, H., 1988. Isotope dilution mass spectrometry. In: Adams, F., Gijbels, R., Van Greiken, R. (Eds.), Inorganic Mass Spectrometry. Wiley Interscience, New York, pp. 301–376.

Hou, Z., Ma, H., Khin, Z., Zhang, Y., Wang, M., Wang, Z., Pan, G., and Tang, R., 2003, The Himalayan Yulong porphyry copper belt: Product of large-scale strike-slip faulting in eastern Tibet: Economic Geology, v. 98, p. 125-145.

Hou, Z., Zeng, P., Gao, Y., Du, A., and Fu, D., 2006, Himalayan Cu-Mo-Au mineralization in the eastern Indo-Asian collision zone: constraints from Re-Os dating of molybdenite: Mineralium Deposita, v. 41, p. 33-45.

Jackson, S. E., Pearson, N. J., Griffin, W. L., and Belousova, E. A., 2004, The application of laser ablation-inductively coupled plasma-mass spectrometry to in situ U-Pb zircon geochronology: Chemical Geology, v. 211, p. 47-69.

Kosler, J., Simonetti, A., Sylvester, P. J., Cox, R. A., Tubrett, M. N., and Wilton, D., 2003, Laser-ablation ICP-MS measurements of Re-Os in molybdenite and implications for Re-Os geochronology: Canadian Mineralogist, v. 41, p. 307-320.

Lawley, C. J. M., and Selby, D., 2012, Re-Os geochronology of quartz-enclosed ultrafine molybdenite: Implications for ore deposit geology: Economic Geology, v. 107, p. 1499-1505.

Li, J., Qin, K., Li, G., Cao, M., Xiao, B., Chen, L., Zhao, J., Evans, N. J., and McInnes, B. I. A., 2012, Petrogenesis and thermal history of the Yulong porphyry copper deposit, Eastern Tibet: insights from U-Pb and U-Th/He dating, and zircon Hf isotope and trace element analysis: Mineralogy and Petrology, v. 105, p. 201-221.

Li, X., Liu, X., Liu, Y., Su, L., Sun, W., Huang, H., and Yi, K., 2015, Accuracy of LA-ICPMS zircon U-Pb age determination: An inter-laboratory comparison: Science China Earth Sciences, v. 58, p. 1722-1730.

Li, Y., Selby, D., Condon, D., Tapster, S., 2017. Cyclic magmatic-hydrothermal evolution in porphyry systems: High-precision U-Pb and Re-Os geochronology constraints from the Tibetan Qulong porphyry Cu-Mo deposit. Economic Geology, in press.

Liang, H., Campbell, I. H., Allen, C., Sun, W., Liu, C., Yu, H., Xie, Y., and Zhang, Y., 2006, Zircon Ce^{4+}/Ce^{3+} ratios and ages for Yulong ore-bearing porphyries in eastern Tibet: Mineralium Deposita, v. 41, p. 152-159.

Liang, H., Mo, J., Sun, W., Yu, H., Zhang, Y., and M, A. C., 2008, Study on the duration of the ore-forming system of the Yulong giant porphyry copper deposit in eastern Tibet, China: Acta Petrologica Sinica, v. 24, p. 2352-2358.

Liu, Y., Hu, Z., Zong, K., Gao, C., Gao, S., Xu, J., and Chen, H., 2010, Reappraisement and refinement of zircon U-Pb isotope and trace element analyses by LA-ICP-MS: Chinese Science Bulletin, v. 55, p. 1535-1546.

Ludwig, K. R., 2003, User's manual for Isoplot 3.00: a geochronological toolkit for Microsoft Excel, Kenneth R. Ludwig.

Ma, H. W., 1990, Petrology and mineralization of granites in Yulong porphyry copper belt, Tibet, China University of Geosciences Press, Wuhan, 107 p.

Markey, R., Stein, H., Hannah, J.L., Zimmerman, A., Selby, D., Creaser, R.A., 2007. Standardizing Re-Os geochronology: a new molybdenite Reference Material (Henderson, USA) and the stoichiometry of Os salts. *Chemical Geology*, 244, 74-87.

Maksaev, V., Munizaga, F., McWilliams, M., Fanning, M., Mathur, R., Ruiz, J., and Zentilli, M., 2004, New chronology for El Teniente, Chilean Andes, from U-Pb, $^{40}Ar/^{39}Ar$, Re-Os and fission-track dating: implications for the evolution of a supergiant porphyry Cu-Mo deposit: Society of Economic Geologists Special Publication, v. 11, p. 15-54.

Meyer, C., and Hemley, J.J., 1967, Wall rock alteration, in Barnes, H.L., ed., Geochemistry of hydrothermal ore deposits: New York, Holt, Rinehart and Winston, p. 166−235.

Porter, S. J., and Selby, D., 2010, Rhenium-Osmium (Re-Os) molybdenite systematics and geochronology of the Cruachan Granite skarn mineralization, Etive Complex: implications for emplacement chronology: Scottish Journal of Geology, v. 46, p. 17-21.

Reiners, P. W., 2005, Zircon (U-Th)/He thermochronometry: Reviews in Mineralogy and Geochemistry, v. 58, p. 151-179.

Richards, J. P., 2013, Giant ore deposits formed by optimal alignments and combinations of geological processes: Nature Geoscience, v. 6, p. 911-916.

Schaltegger, U., Schmitt, A. K., and Horstwood, M. S. A., 2015, U-Th-Pb zircon geochronology by ID-TIMS, SIMS, and laser ablation ICP-MS: Recipes, interpretations, and opportunities: Chemical Geology, v. 402, p. 89-110.

Seedorff, E., Dilles, J. H., Proffett, J. M., Einaudi, M. T., Zurcher, L., Stavast, W., Johnson, D. A., and Barton, M. D., 2005, Porphyry deposits: characteristics and origin of hypogene features: Economic Geology 100th Anniversary Volume, v. 29, p. 251-298.

Selby, D., Creaser, R. A., Stein, H. J., Markey, R. J., and Hannah, J. L., 2007, Assessment of the ^{187}Re decay constant by cross calibration of Re-Os molybdenite and U-Pb zircon chronometers in magmatic ore systems: Geochimica et Cosmochimica Acta, v. 71, p. 1999-2013.

Selby, D., and Creaser, R. A., 2001, Re-Os geochronology and systematics in molybdenite from the Endako porphyry molybdenum deposit, British Columbia, Canada: Economic Geology, v. 96, p. 197-204.

Selby, D., Creaser, R.A., Heaman, L.M., and Hart, C.J.R., 2003. Re-Os and U-Pb geochronology of the Clear Creek, Dublin Gulch and Mactung deposits, Tombstone Gold Belt, Canada: Absolute timing relationships between plutonism and mineralization. Canadian Journal of Earth Sciences, v. 40, p. 1839-1852.

Selby, D., Creaser, R.A., and Feely, M., 2004. Accurate and precise Re-Os molybdenite dates from the Galway Granite, Ireland. A Critical Comment to: "Disturbance of the Re-Os chronometer of molybdenites from the late-Caledonian Galway Granite, Ireland, by hydrothermal fluid circulation." *Geochemical Journal*, v. 35, p. 29-35.

Selby, D., and Creaser, R. A., 2004, Macroscale NTIMS and microscale LA-MC-ICP-MS Re-Os isotopic analysis of molybdenite: Testing spatial restrictions for reliable Re-Os age determinations, and implications for the decoupling of Re and Os within molybdenite: Geochimica et Cosmochimica Acta, v. 68, p. 3897-3908.

Sillitoe, R. H., 2010, Porphyry copper systems: Economic Geology, v. 105, p. 3-41.

Sillitoe, R. H., and Mortensen, J. K., 2010, Longevity of porphyry copper formation at Quellaveco, Peru: Economic Geology, v. 105, p. 1157-1162.

Simmons, S. F., and Brown, K. L., 2006, Gold in Magmatic Hydrothermal Solutions and the Rapid Formation of a Giant Ore Deposit: Science, v. 314, p. 288-291.

Smoliar, M. I., Walker, R. J., and Morgan, J. W., 1996, Re-Os ages of group IIA, IIIA, IVA, and IVB iron meteorites: Science, v. 271, p. 1099.

Spencer, E. T., Wilkinson, J. J., Creaser, R. A., and Seguel, J., 2015, The Distribution and Timing of Molybdenite Mineralization at the El Teniente Cu-Mo Porphyry Deposit, Chile: Economic Geology, v. 110, p. 387-421.

Stein, H. J., 2006, Low-rhenium molybdenite by metamorphism in northern Sweden: recognition, genesis, and global implications: Lithos, v. 87, p. 300-327.

Stein, H. J., 2014, Dating and tracing the history of ore formation, in Turekian, K.K., Holland, H.D., and Scott, S.D., eds., Treatise on geochemistry, 2nd edition, v. 12 (Mineral Resources), Oxford, Elsevier-Pergamon, p. 88-118.

Stein, H. J., Sundblad, K., Markey, R. J., Morgan, J. W., and Motuza, G., 1998, Re-Os ages for Archean molybdenite and pyrite, Kuittila-Kivisuo, Finland and Proterozoic molybdenite, Kabeliai, Lithuania: testing the chronometer in a metamorphic and metasomatic setting: Mineralium Deposita, v. 33, p. 329-345.

Stein, H., Scherstén, A., Hannah, J., and Markey, R., 2003, Subgrain-scale decoupling of Re and ^{187}Os and assessment of laser ablation ICP-MS spot dating in molybdenite: Geochimica et Cosmochimica Acta, v. 67, p. 3673-3686.

Tang, J. X., 2003, The study on metallogeny and localizing forecast of Yulong porphyry copper-molybdenum mineralization, Tibet: Unpublished Ph.D. thesis, Chengdu, China, Chengdu University of Technology, 46 p.

Tang, J. X., Wang, C. H., Qu, W. J., Du, A. D., Ying, L. J., and Gao, Y. M., 2009, Re-Os isotopic dating of molybdenite from the Yulong porphyry copper-molybdenum deposit in Tibet and its metallogenic significance: Rock and Mineral Analysis, v. 28, p. 215-218.

Tang, R. L., and Luo, H. S., 1995, The geology of Yulong porphyry copper (molybdenum) ore belt, Xizang (Tibet), Geological Publishing House, Beijing, 157 p.

von Quadt, A., Erni, M., Martinek, K., Moll, M., Peytcheva, I., and Heinrich, C. A., 2011, Zircon crystallization and the lifetimes of ore-forming magmatic-hydrothermal systems: Geology, v. 39, p. 731-734.

Vry, V. H., Wilkinson, J. J., Seguel, J., and Millán, J., 2010, Multistage intrusion, brecciation, and veining at El Teniente, Chile: Evolution of a nested porphyry system: Economic Geology, v. 105, p. 119-153.

Wang, C. H., Tang, J. X., Chen, J. P., Hao, J. H., Gao, Y. M., Liu, Y. W., Fan, T., Zhang, Q. Z., Ying, L. J., and Chen, Z. J., 2009, Chronological research of Yulong copper-molybdenum porphyry deposit: Acta Geologica Sinica, v. 83, p. 1445-1455.

Weis, P., Driesner, T., and Heinrich, C. A., 2012, Porphyry-copper ore shells form at stable pressure-temperature fronts within dynamic fluid plumes: Science, v. 338, p. 1613-1616.

Wiedenbeck, M., Alle, P., Corfu, F., Griffin, W. L., Meier, M., Oberli, F., Quadt, A. V., Roddick, J. C., and Spiegel, W., 1995, Three natural zircon standards for U-Th-Pb, Lu-Hf, trace element and REE analyses: Geostandards newsletter, v. 19, p. 1-23.

Wilkinson, J. J., 2013, Triggers for the formation of porphyry ore deposits in magmatic arcs: Nature Geoscience, v. 6, p. 917-925.

Zhang, Y., and Xie, Y., 1997, Geochronology of Ailaoshan-Jinshajiang alkali-rich intrusive rocks and their Sr and Nd isotopic characteristics: Science in China Series D: Earth Sciences, v. 40, p. 524-529.

Figure and table captions

Figure 1. Regional and local geology of the Yulong porphyry Cu-Mo deposit in eastern Tibet. A. Simplified geologic map of the Eocene Yulong porphyry Cu belt showing distribution of the volcanic rocks, porphyry copper deposits (in red) and weakly mineralized porphyries (in black) (modified from Hou et al., 2003). The ages of the volcanic rocks and porphyries are compiled from Zhang and Xie (1997), Wang et al. (2000), Hou et al. (2003), and Liang et al. (2006). The location of the Yulong porphyry Cu belt is shown in the insert. B. Local geology of the Yulong deposit and surrounding areas (modified from an unpublished report of the Tibet Yulong Copper Co., Ltd, 2007).

Figure 2. Geologic cross-sections through the Yulong deposit. A. NNW-SSE cross-section C-C` parallel to the elongated Yulong stock. B. ENE-WSW cross-section 9-9` perpendicular to the elongated Yulong stock. Base map of the sections and the Cu and Mo grade data are taken from an unpublished report (Tibet Yulong Copper Co., Ltd., 2009). Note the distribution of the KGP and QAP revealed by the drill holes. Sampling locations for zircon U-Pb and molybdenite Re-Os dating are indicated. Locations of the sections are shown in Figure 1B.

Figure 3. Summary of the previously published zircon U-Pb, molybdenite Re-Os and zircon and apatite (U-Th)/He data for the Yulong deposit and the surrounding barren porphyries (Guo et al., 2006; Hou et al., 2006; Liang et al., 2006; Tang et al., 2009; Wang et al., 2009; Li et al., 2012). Zircon U-Pb ages from Liang et al. (2006) and Li et al. (2012) are weighted mean of $^{206}Pb/^{238}U$ dates of several dated MGP samples in the same papers, and the molybdenite Re-Os age is a weighted mean of model ages from Hou et al. (2006) and Tang et al. (2009). The others are original data from corresponding references.

Figure 4. Photographs showing the geologic relations of major porphyries and vein assemblages described in the study. A. Contact between the MGP and KGP, both porphyries exhibiting potassic alteration (sample 1103-432). The quartz vein hosted in the MGP is truncated by the KGP. In addition, both quartz ($A1_T$) and biotite (EB_T) veins cut through the contact between the two porphyries and the K-feldspar vein (ksp)

in the KGP. B. The MGP truncated by the QAP revealed in sample 1205-338. The quartz vein ($A2_E$ vein) in the MGP contains both chalcopyrite and molybdenite. A pyrite vein (D_L) crosscuts the contact between the two porphyries. Green to yellow color of plagioclase phenocrysts in both porphyries reflects the intermediate argillic alteration. Note the unaltered K-feldspar megacrysts. C. Unidirectional solidification textures (USTs) in the KGP close to the contact with the MGP (sample 0607-390). Quartz layers of the USTs are truncated by a barren quartz vein ($A1_T$), and both the USTs and $A1_T$ vein are subsequently cut by a molybdenite-rich quartz vein (B_T vein). The KGP with strong potassic alteration (fine-grained K-feldspar matrix) is overprinted by supergene kaolinite alteration. D. Intrusive contact between KGP and QAP recorded in sample 1103-430. The $A1_T$ vein in the KGP is truncated by the QAP. All scale bars are 1 cm.

Figure 5. Drill hole logs showing lithology, alteration, quartz vein density and Cu, Mo and sulfur grades revealed from two selected diamond drill holes ZK0908 (A) and ZK1103 (B). Copper grade in the KGP is commonly lower than 0.5 wt%, whereas Mo grade can reach up to 0.1 wt%. QAP dikes are associated with intense to strong sericitic alteration. Note the low quartz vein density and high sulfur grade of the QAP in drill hole ZK1103 @ 405 m.

Figure 6. Photographs showing crosscutting relationships of various vein types. A. Magnetite-bearing quartz veins (M_E vein) cut by a barren quartz vein ($A1_E$ vein) in potassic altered MGP (sample 1303-789). B. A quartz-biotite vein (EB_E vein) truncated by a $A1_E$ vein in MGP (sample 1303-771). Note the intermediate argillic alteration formed by consuming plagioclase phenocrysts (pale green). C. A discontinuous $A1_E$ vein cut by a thin EB_E and a quartz-molybdenite ± pyrite vein (B_T vein) in MGP (sample 1303-966). Pyrite in the EB_E vein is interpreted as an overprint. The pale green color of plagioclase phenocrysts is caused by intermediate argillic alteration. D. Quartz-molybdenite ± chalcopyrite veins ($A2_E$ vein) cut by EB_E veins (sample 1303-114). The white and powdery appearance of plagioclase phenocrysts reflects supergene kaolinite leaching. E. $A2_E$ veins cut by a chalcopyrite ±

pyrite-dominated $A3_E$ veinlet in the MGP (sample 1303-158). Note the contrasting size and appearance of the vein quartz xenolith (xnl) and quartz phenocrysts (phc). F. Crosscutting relationships of three typical $A2_E$ veins in the MGP (sample 1303-115). G. A $A2_E$ vein reopened and filled by a sulfide-dominated $A3_E$ vein in the MGP (sample 0905-207). H. Rarely observed sulfide-dominated $A3_T$ vein in the KGP (sample 1103-437). I. Sequential formation of $A2_E$, B_T and D_L veins verified by the crosscutting relationships in the intensely sericitic altered MGP (sample 1007-414). See Table 2 for mineral abbreviations. All scale bars are 1 cm.

Figure 7. Photographs showing various degree of potassic alteration in the MGP. A. Intense potassic alteration marked by complete destruction of phenocrysts and formation of locally abundant quartz-magnetite (M_E) veinlets (sample 0905-445). B. Intense potassic alteration marked by the residues of the MGP in $A1_E$ vein that have been altered to form fine-grained quartz and K-feldspar (sample 0812-141). C. Strong to moderate potassic alteration illustrated by abundant hydrothermal biotite (sample 0904-183). D. Moderate to weak potassic alteration (sample 1303-145). Most crystal edges are visible, but hydrothermal biotite is common. The white and powdery appearance of plagioclase is consistent with supergene kaolinite leaching. See Table 2 for mineral abbreviations. All scale bars are 1 cm.

Figure 8. Distribution of quartz vein density and Cu-Mo mineralization revealed by drill cores along the two perpendicular cross-sections shown in Figure 1B. Note the general decoupling between high quartz vein density and high grade Cu-Mo mineralization. Samples with quartz vein density over 30 vol.% are commonly restricted to the barren core of the MGP. In drill hole ZK1007, intense potassic alteration, however, is manifested by pervasive texture-destructive replacement of the MGP with fine grained K-feldspar and quartz rather than high quartz vein density (see Fig. 7A). The distribution of B_T veins is closely associated with the deep Mo-rich but Cu-poor zone.

Figure 9. Distribution and zonation of hydrothermal alteration based on drill core logging along the two cross-sections shown in Figure 1B. Hydrothermal alteration

generally grades from the intense potassic alteration core outward and upward to strong, moderate, and weak potassic alteration, and outer-propylitic and skarn alteration. The late intense to strong sericitic alteration is dominantly controlled by the emplacement of QAP dikes. Supergene kaolinite alteration in the shallow parts of the deposit destroyed almost all the magmatic and hydrothermal alteration minerals. Hydrothermal alteration out of the range of the logged drill holes is deduced from Du (1980).

Figure 10. Drill hole logs in supergene oxidized skarn ore. Copper grade in the intermediate argillic altered QAP is significantly lower than that in the skarn ore, indicating that the skarn ore formation predates intrusion of the QAP.

Figure 11. Zircon U-Pb concordia diagrams with inset CL images and weighted mean $^{206}Pb/^{238}U$ dates for the MGP, KGP, and QAP. The white circles in the CL images represent the spots of the LA-ICP-MS analyses. The white bars are 100 μm in length for scale.

Figure 12. Photographs showing the occurrences, mineralogical association and textures of $A2_E$ and B_T veins dated in this study as well as the molybdenite Re-Os model ages of individual samples. A-E. $A2_E$ veins in the MGP. F-O. B_T veins hosted by the MGP, KGP and hornfels. Most of these samples have experienced various extent of hydrolytic overprint and/or supergene kaolinite leaching. The coarse-grained molybdenite in sample 0905-159 occurs as fracture infillings of the $A2_E$ vein. The insert in I is a reflected-light photomicrograph showing the molybdenite is paragenetically later than the chalcopyrite in this vein. See Table 2 for mineral abbreviations. Sample numbers are shown on the top or bottom of each photographs.

Figure 13. Schematic illustration of the evolving porphyry intrusions, vein formation, hydrothermal alteration, and Cu-Mo mineralization based on the time line provided by field and texture relationships and Re-Os molybdenite ages (in color). The previous age data and zircon U-Pb ages of this study are also shown for comparison.

Figure 14. The tonnage of selected giant porphyry copper deposits versus duration of

magmatic-hydrothermal processes constrained by high-precision molybdenite Re-Os or ID-TIMS zircon U-Pb dating. Data from von Quadt et al. (2011), Stein (2014), Deckart et al. (2014), Spencer et al. (2015), Buret et al. (2016), Li et al. (in press), and this study.

Table 1. Mineralogical characteristics of Yulong porphyry rock types

Table 2. Paragenetic sequence of vein types at the Yulong porphyry Cu-Mo deposit

Table 3. Re-Os data synopsis for molybdenite from the Yulong porphyry Cu-Mo deposit

APPENDIX 1

Figure A1. The distribution of hydrous minerals in cross-section C-C`. Porphyry intrusions, Cu and Mo grades and field-based alteration zonation are also shown for comparison.

Figure A2. The distribution of hydrous minerals in cross-section 9-9`. Porphyry intrusions, Cu and Mo grades and field-based alteration zonation are also shown for comparison.

APPENDIX 2

Table A1. LA-ICP-MS zircon U-Pb data of porphyry intrusions from the Yulong porphyry Cu-Mo deposit

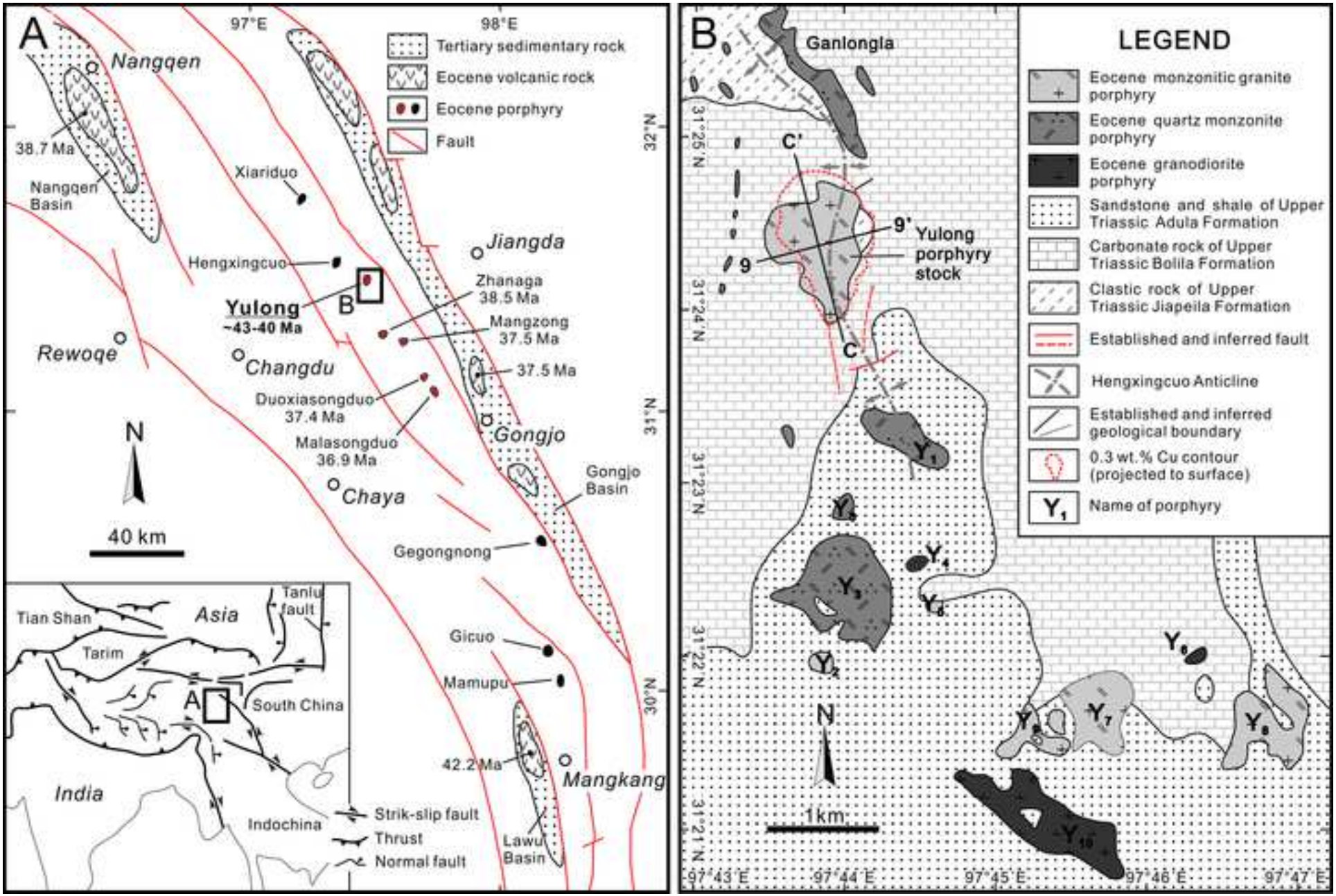

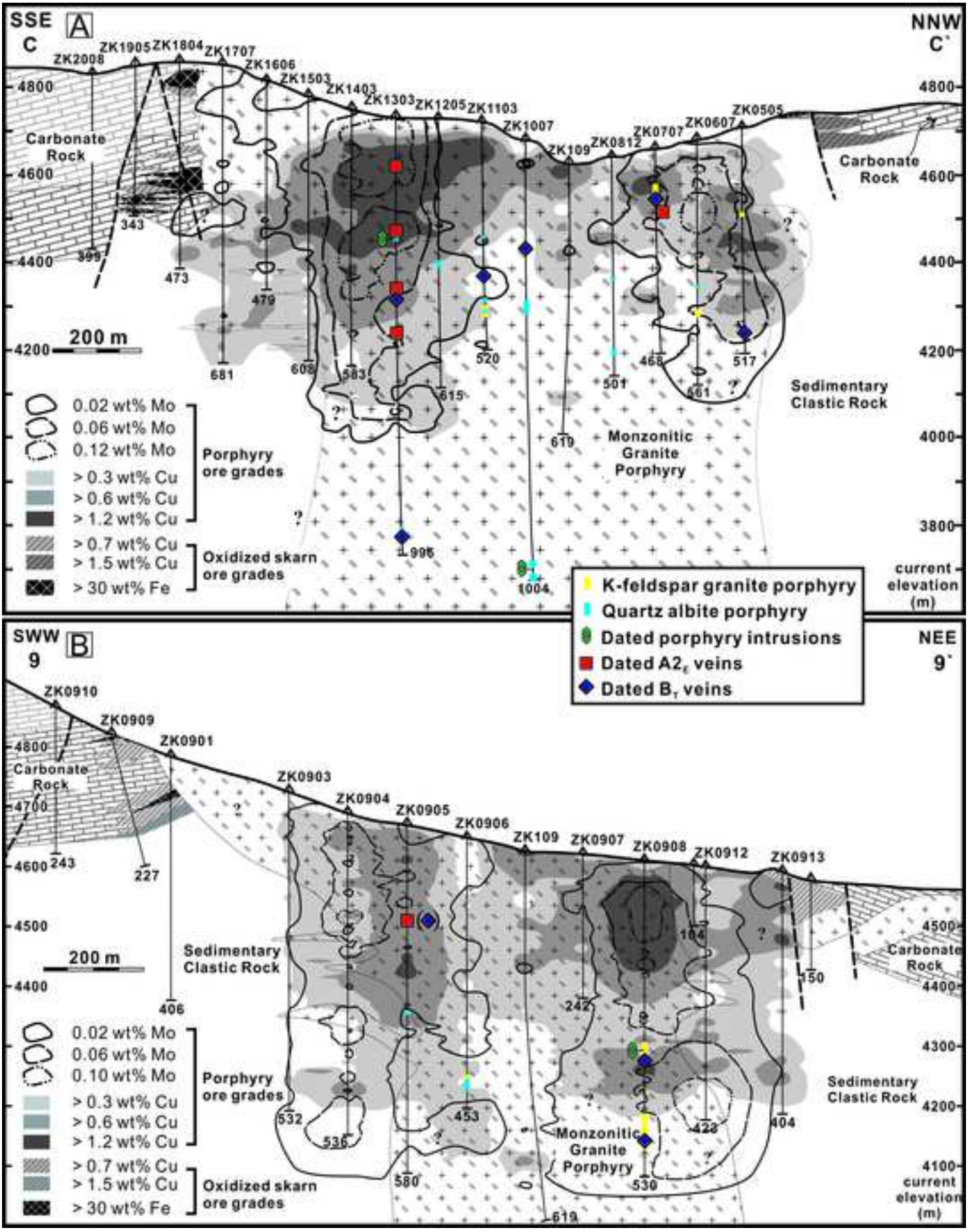

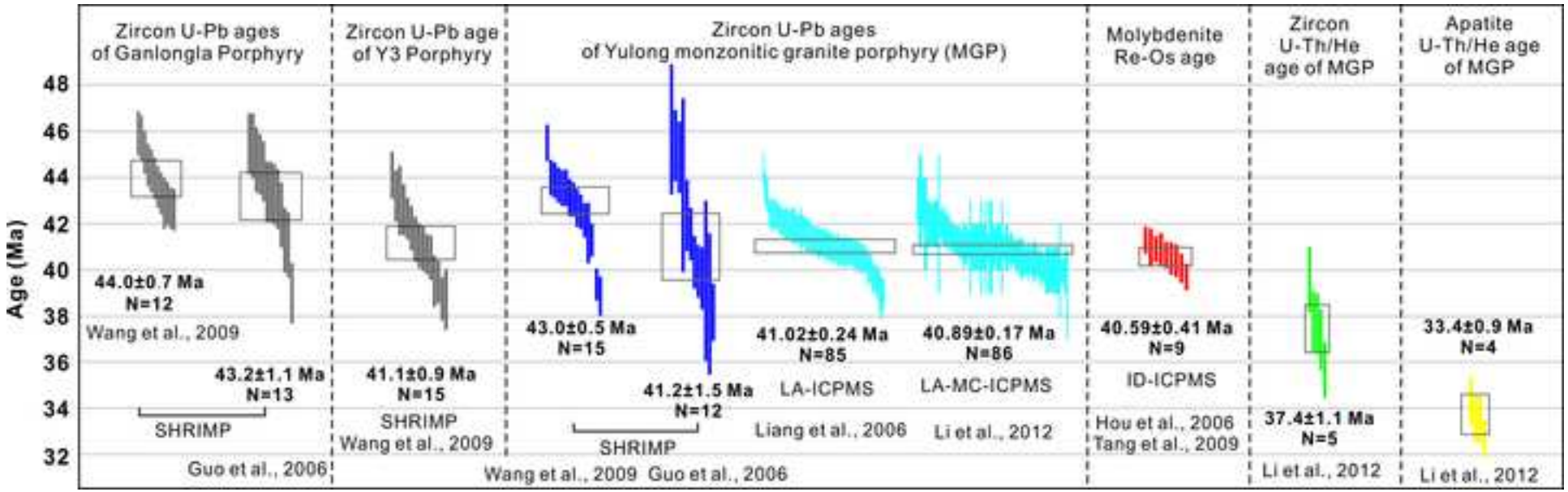

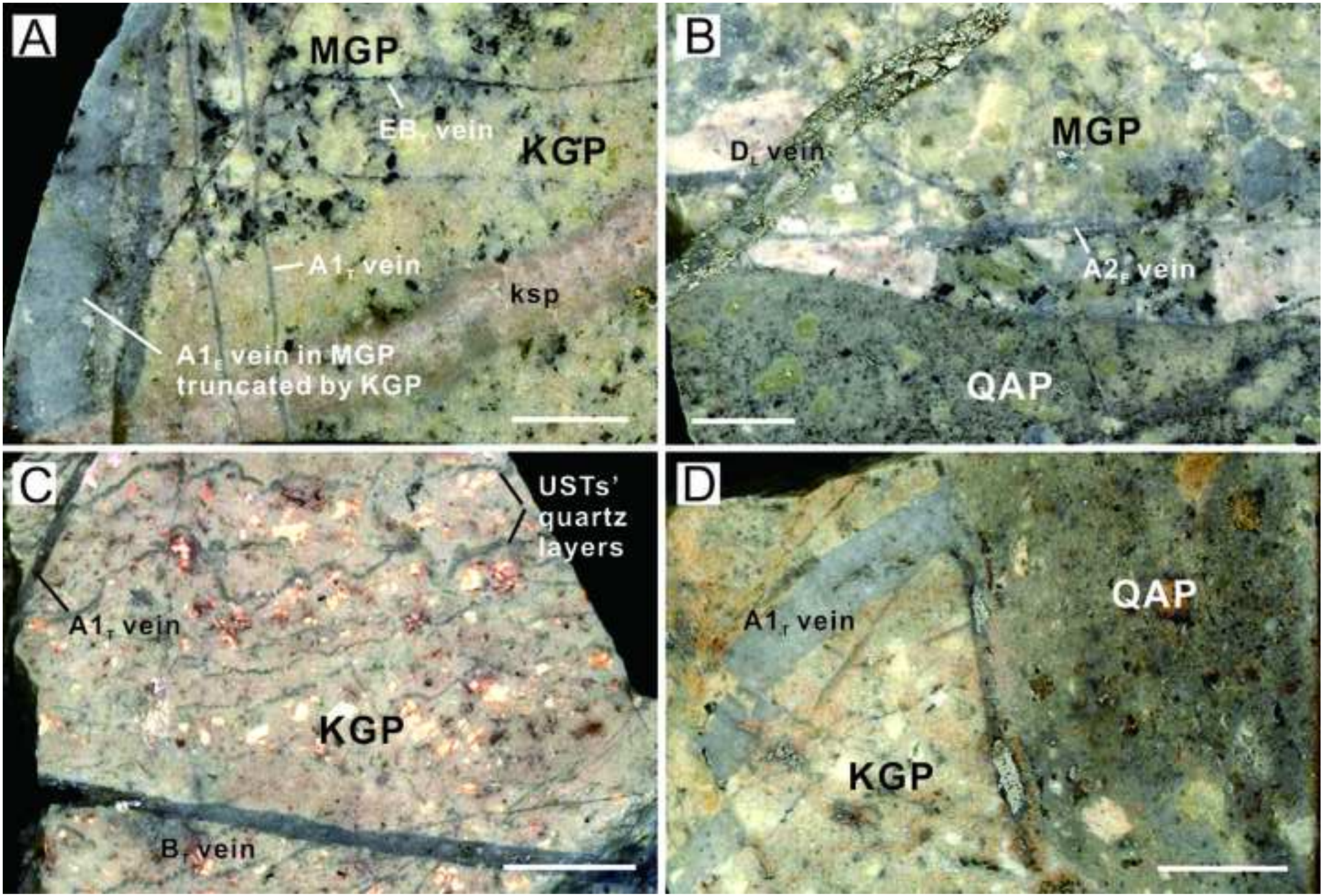

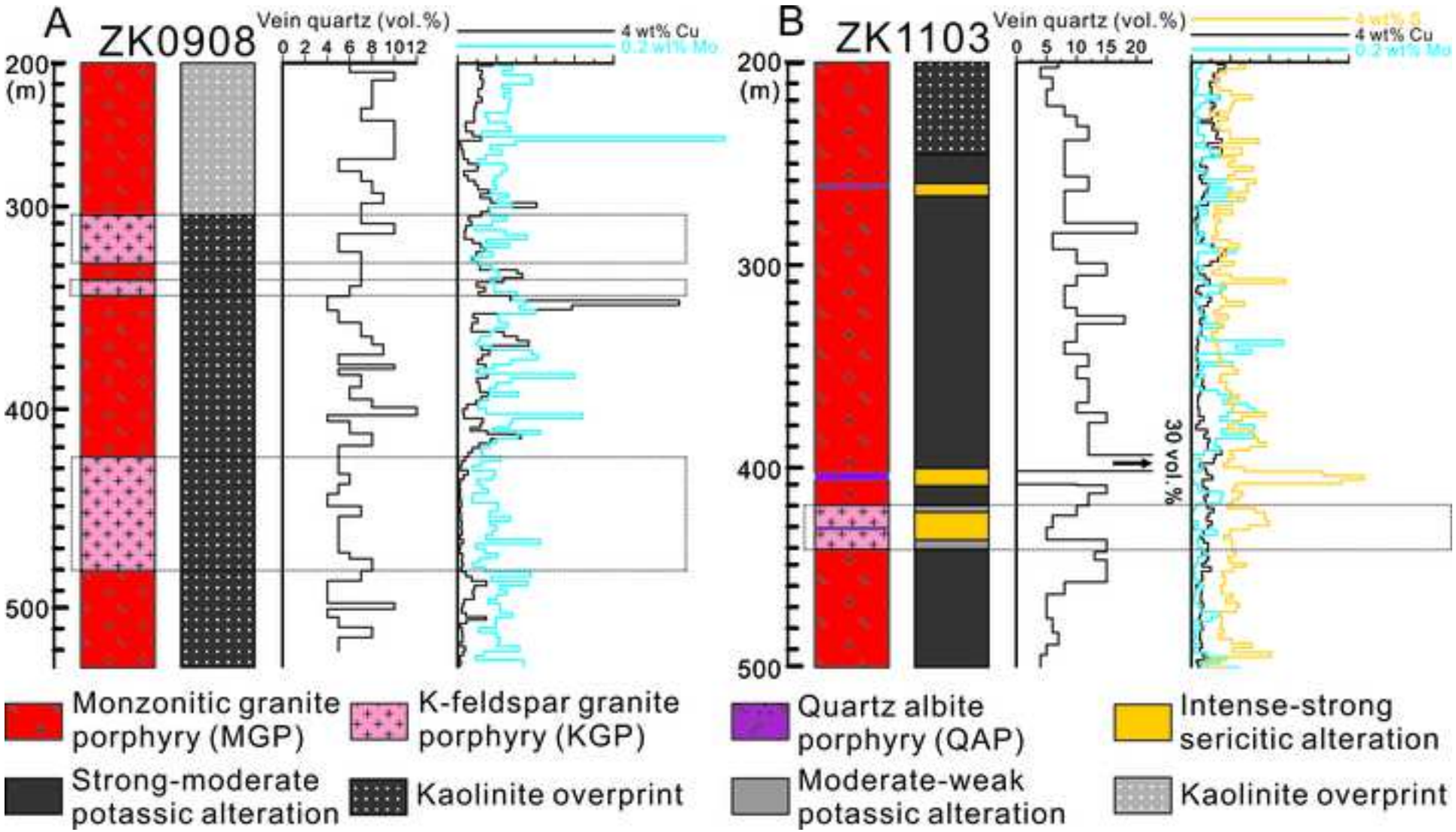

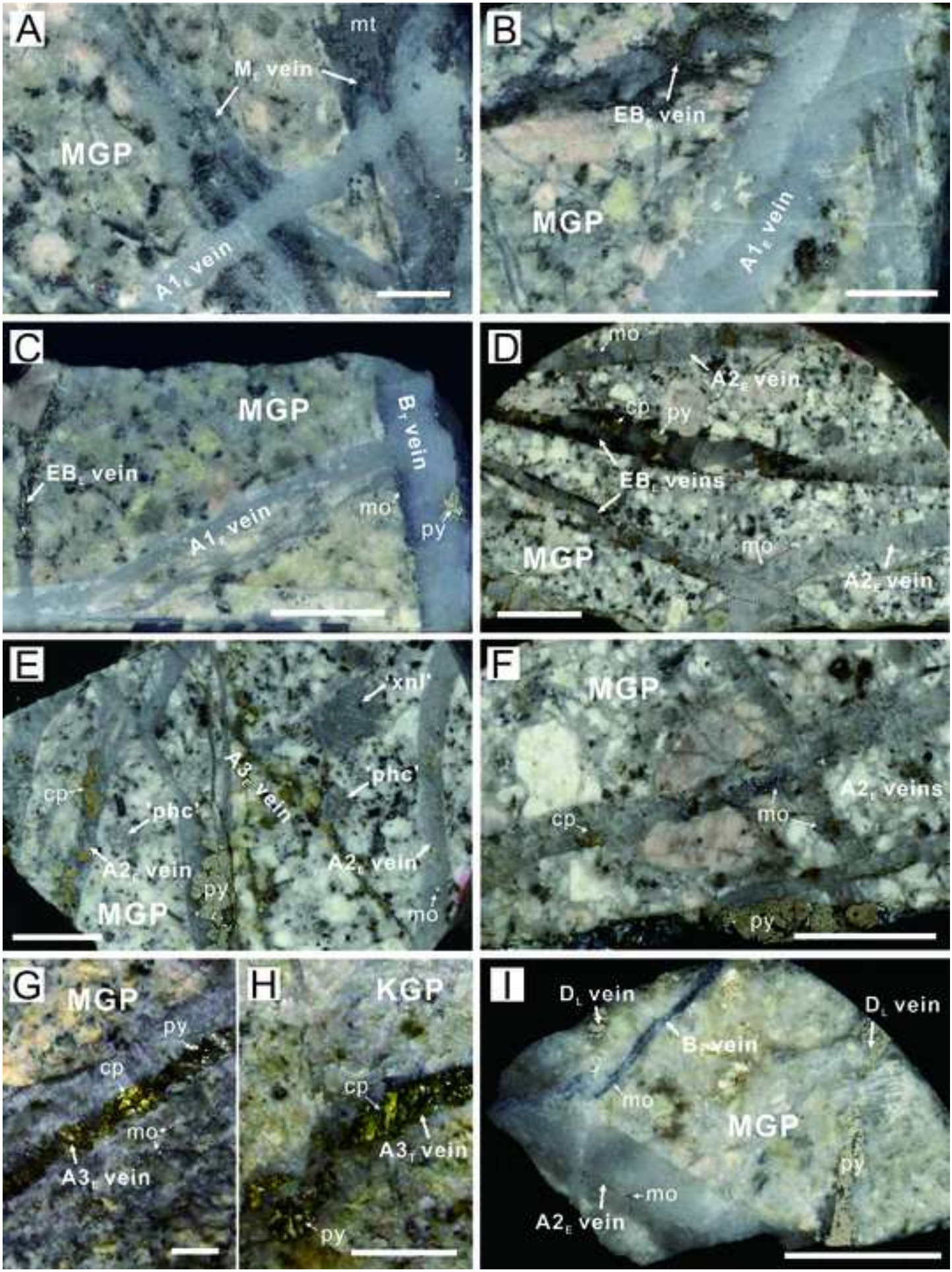

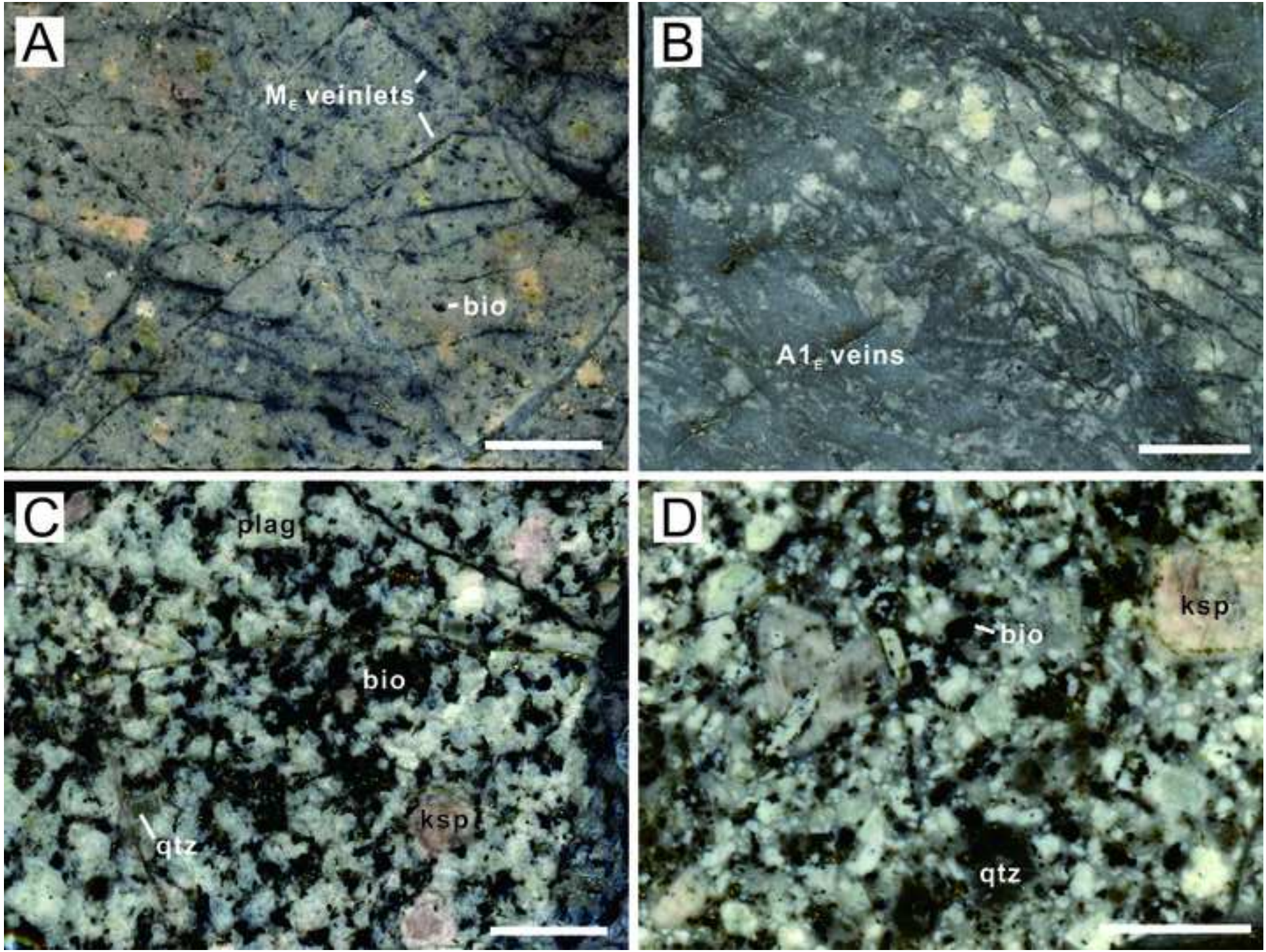

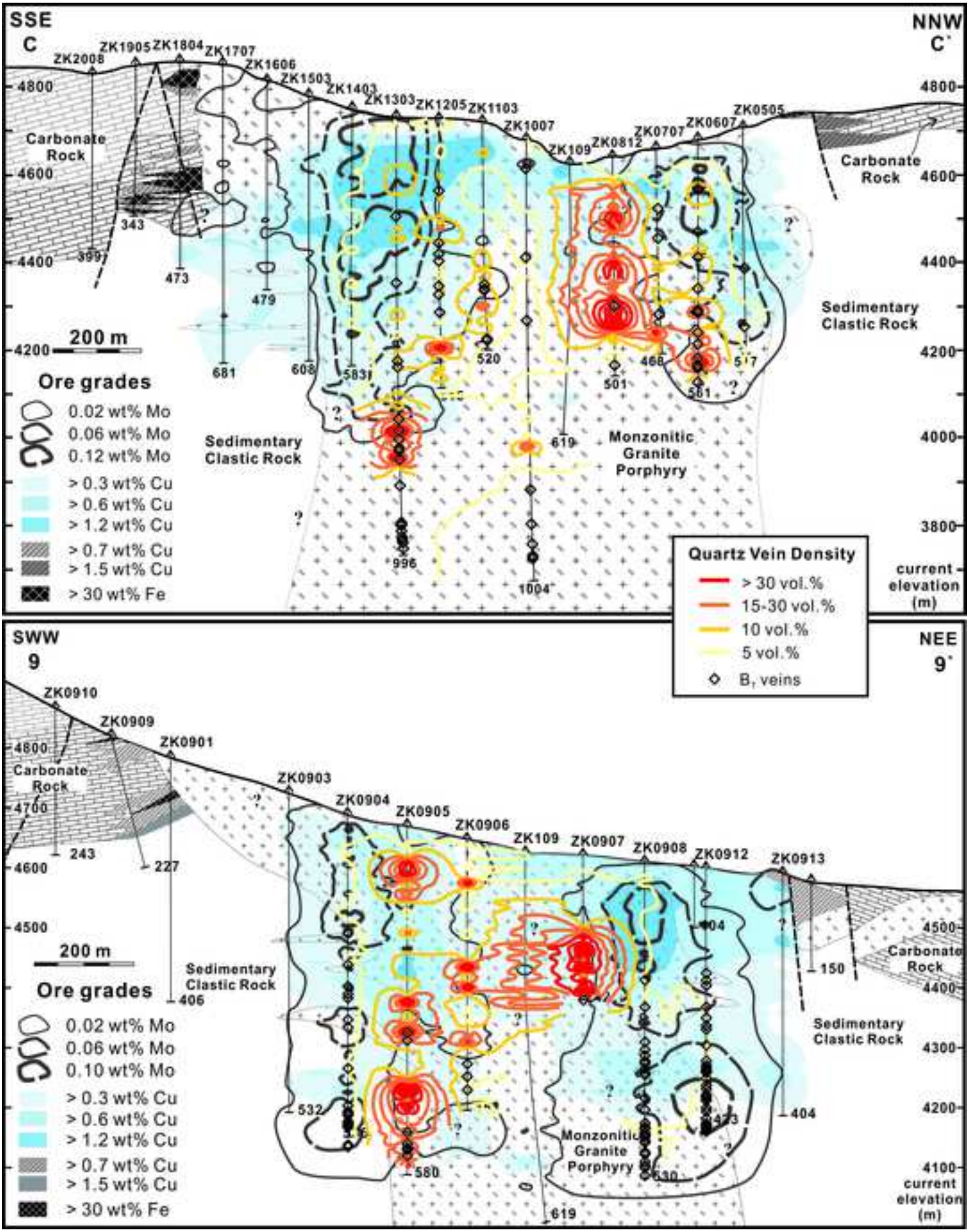

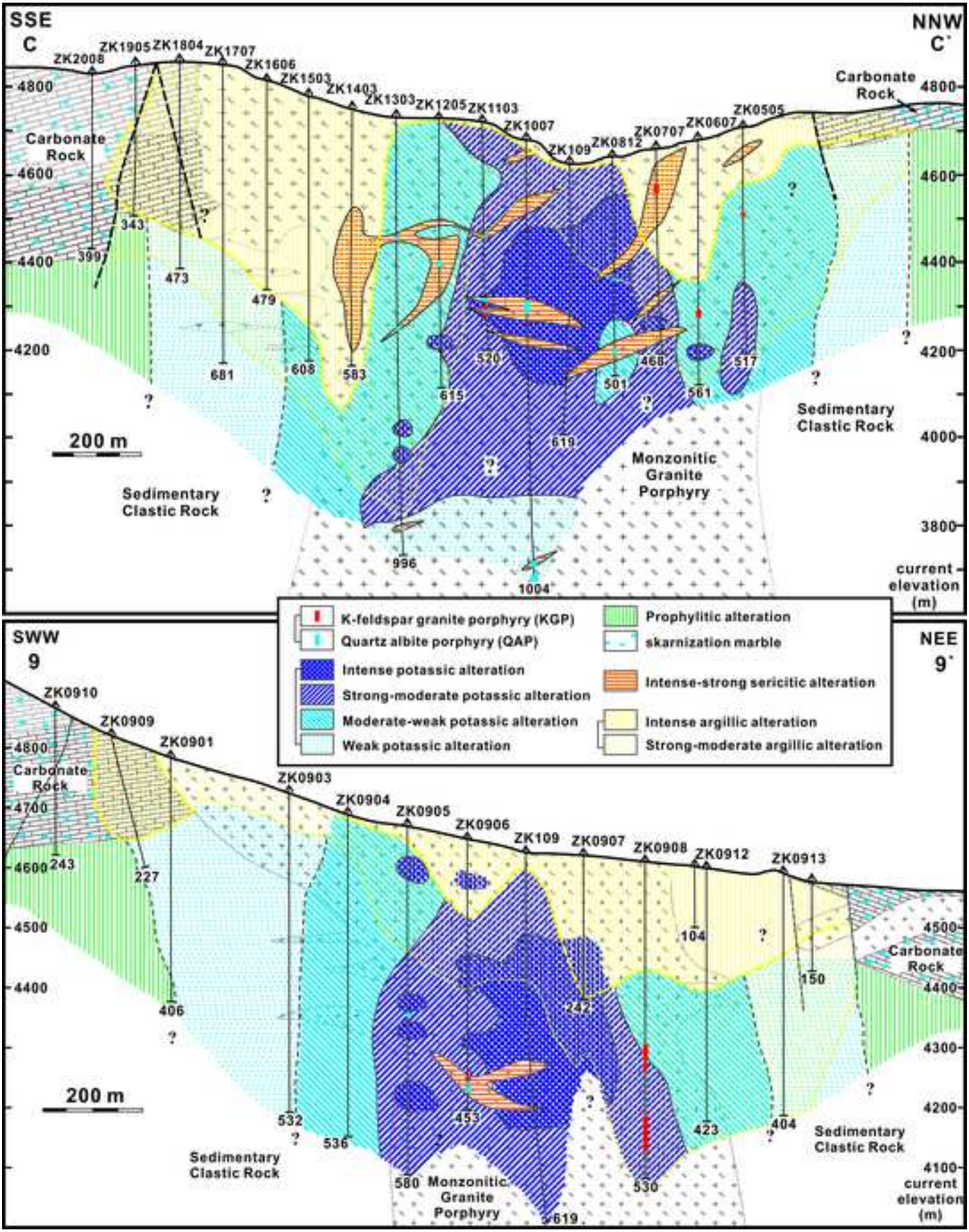

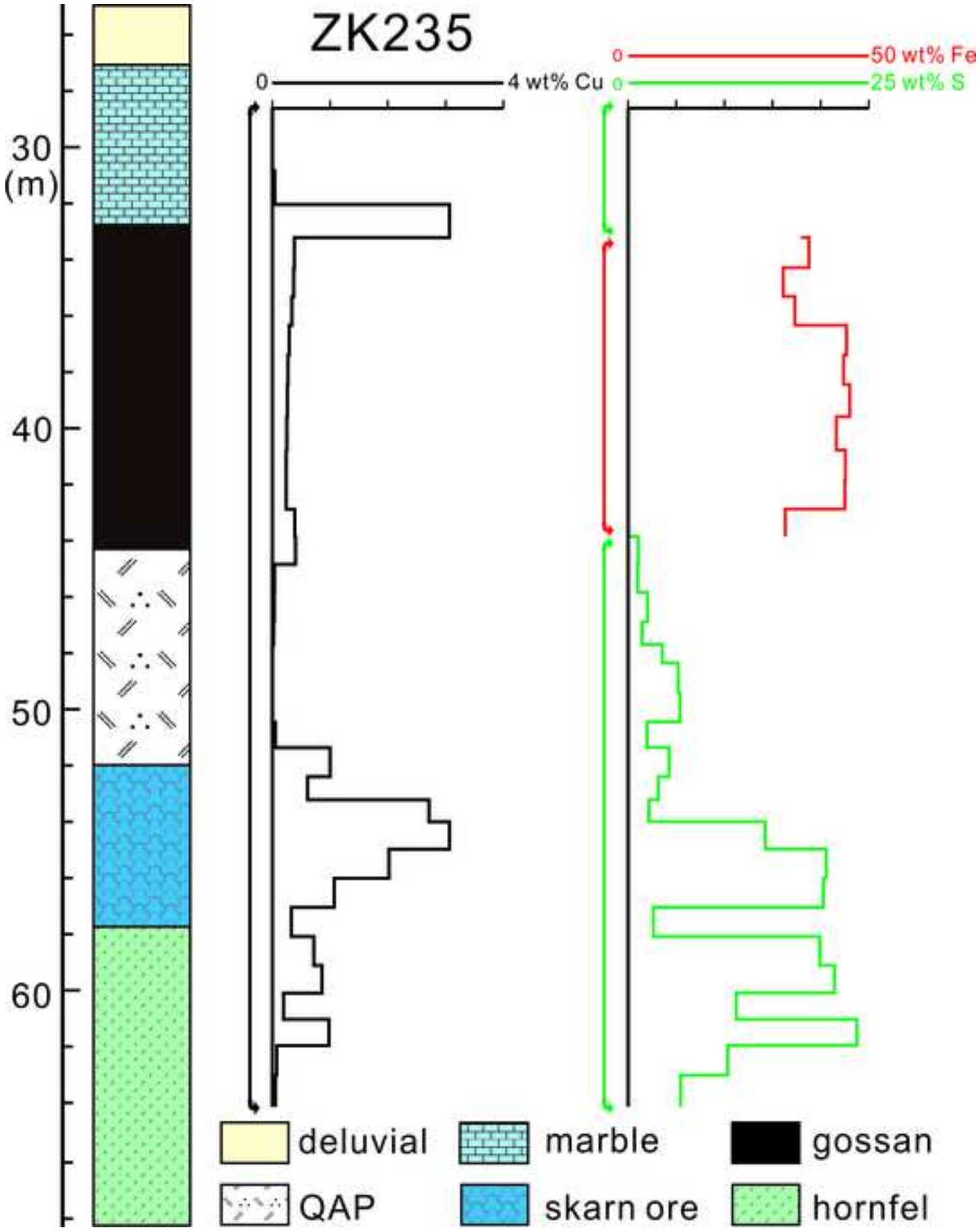

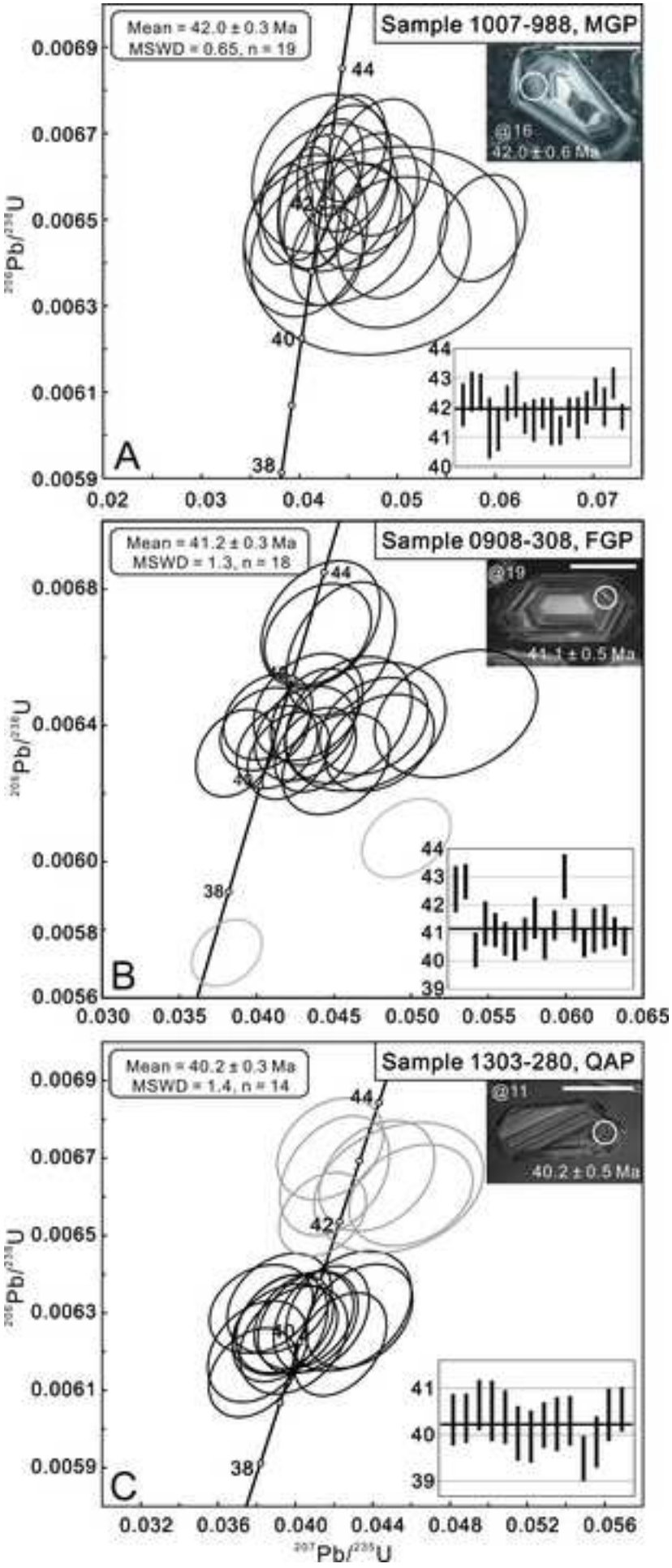

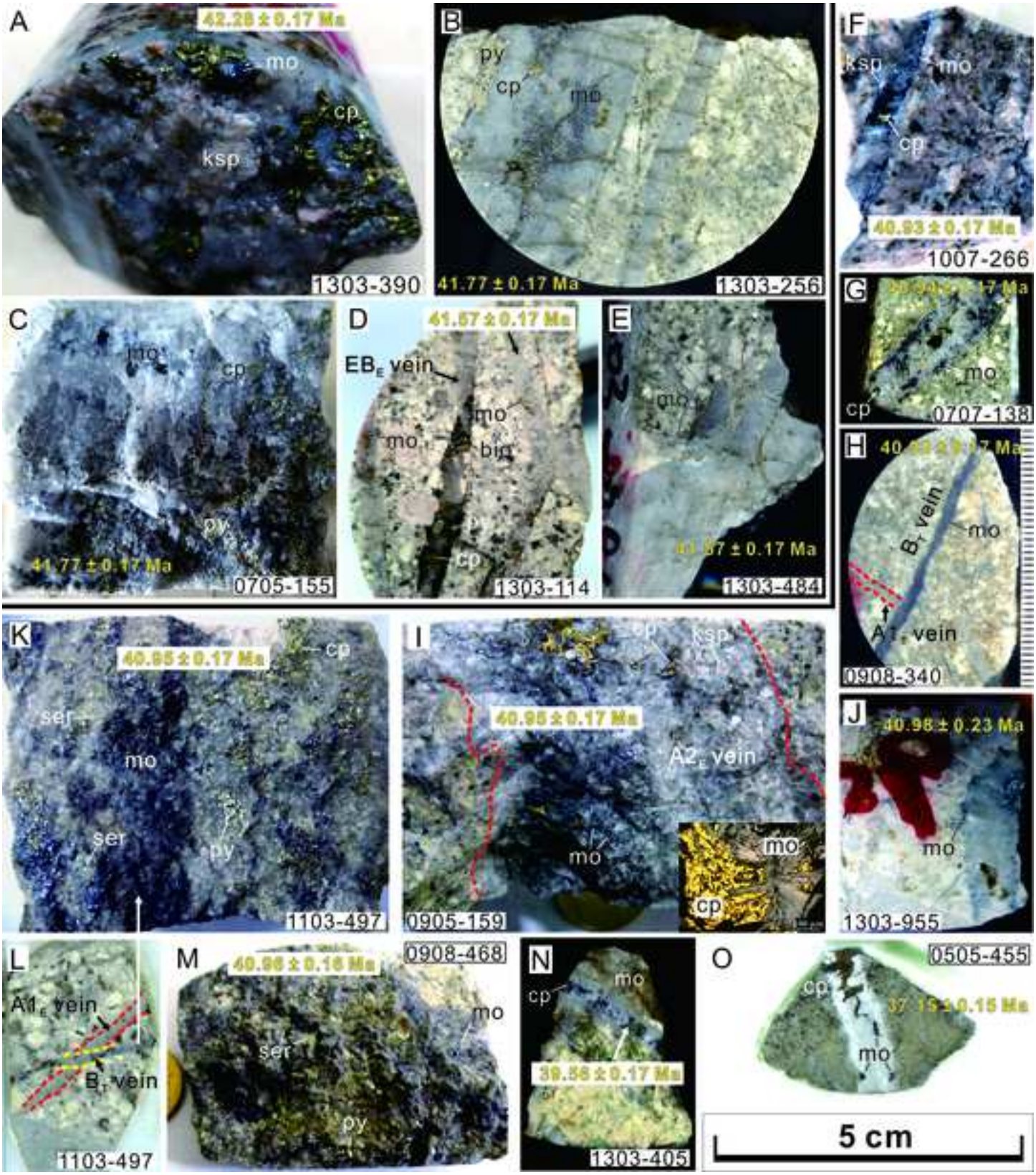

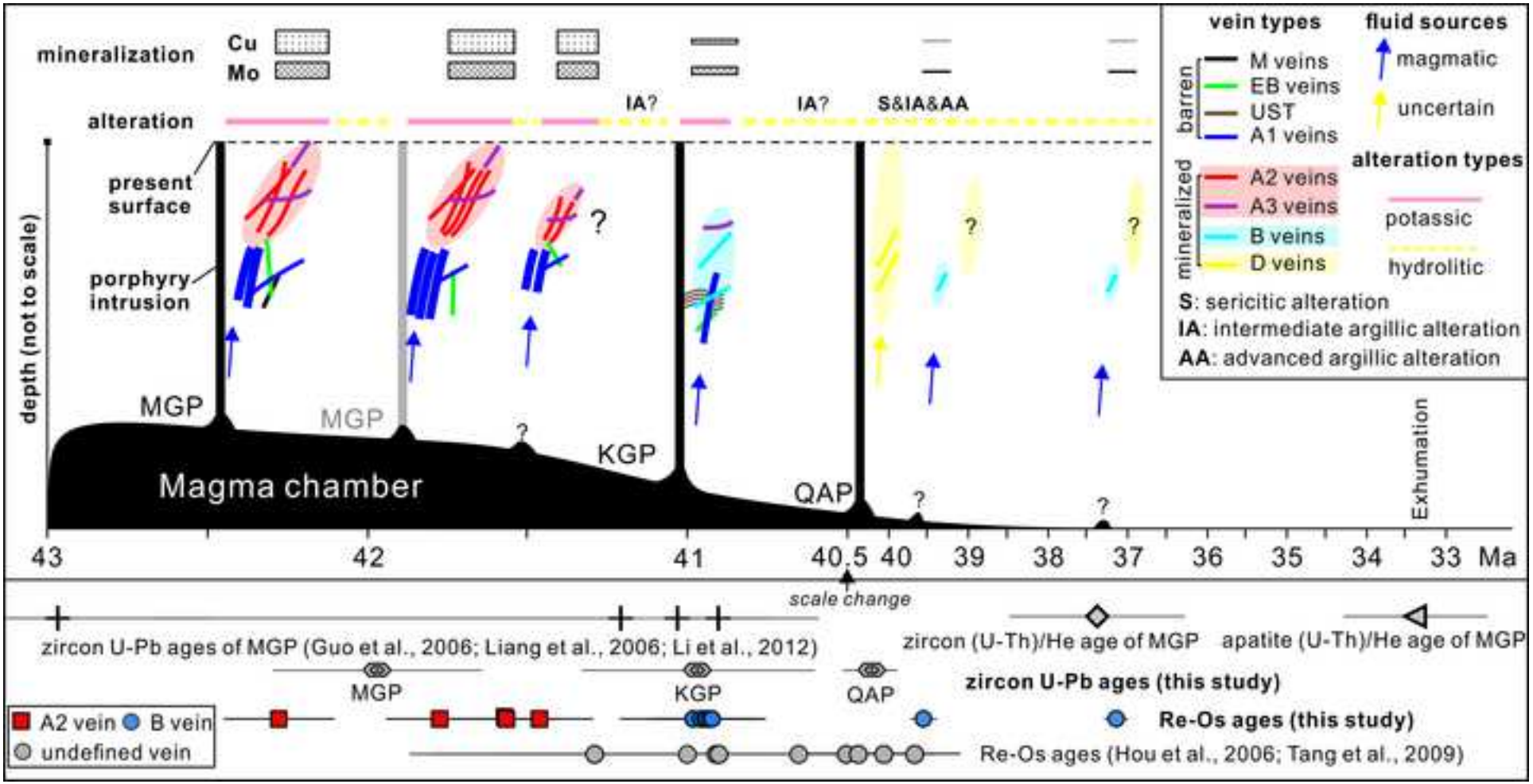

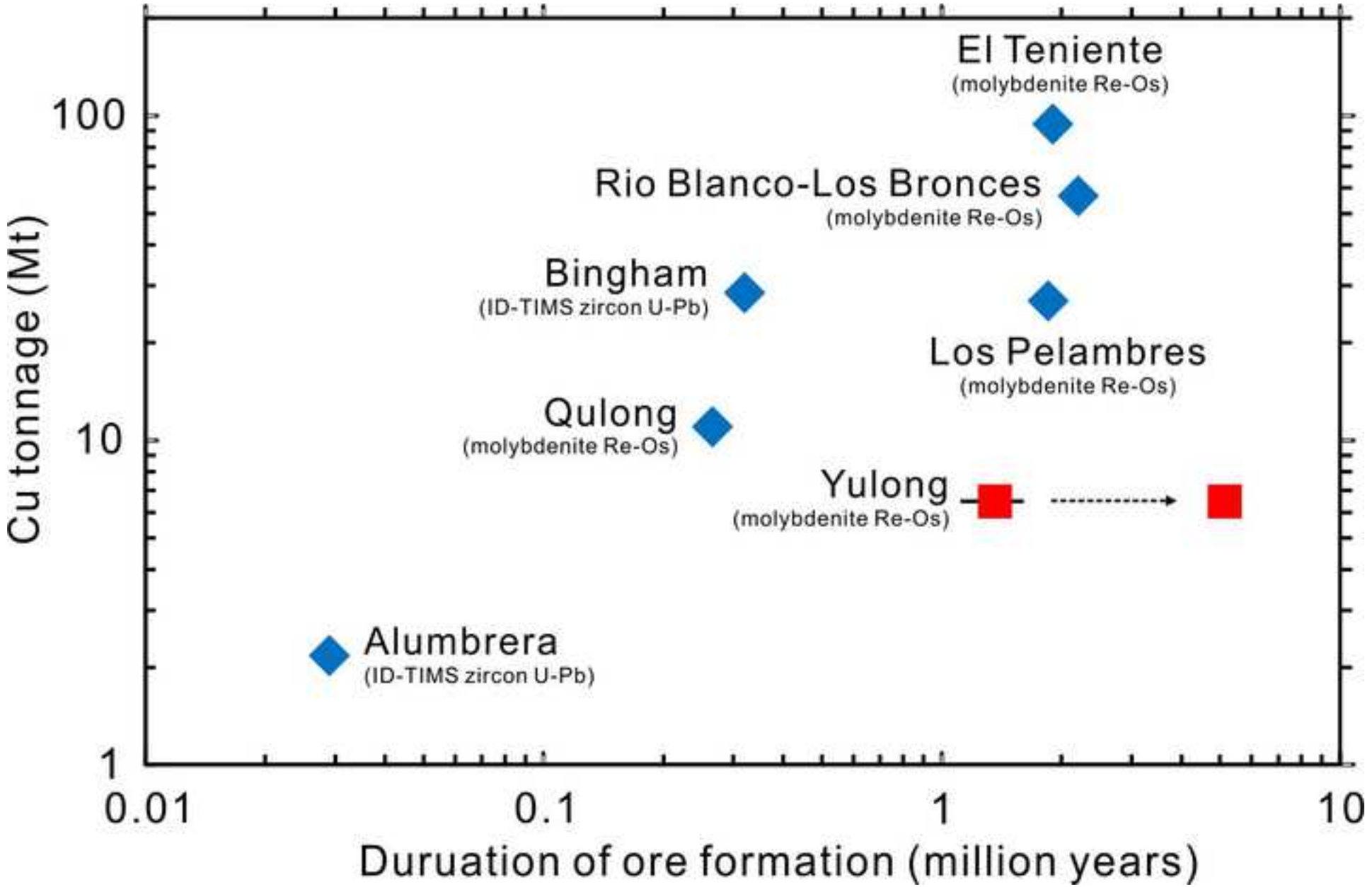

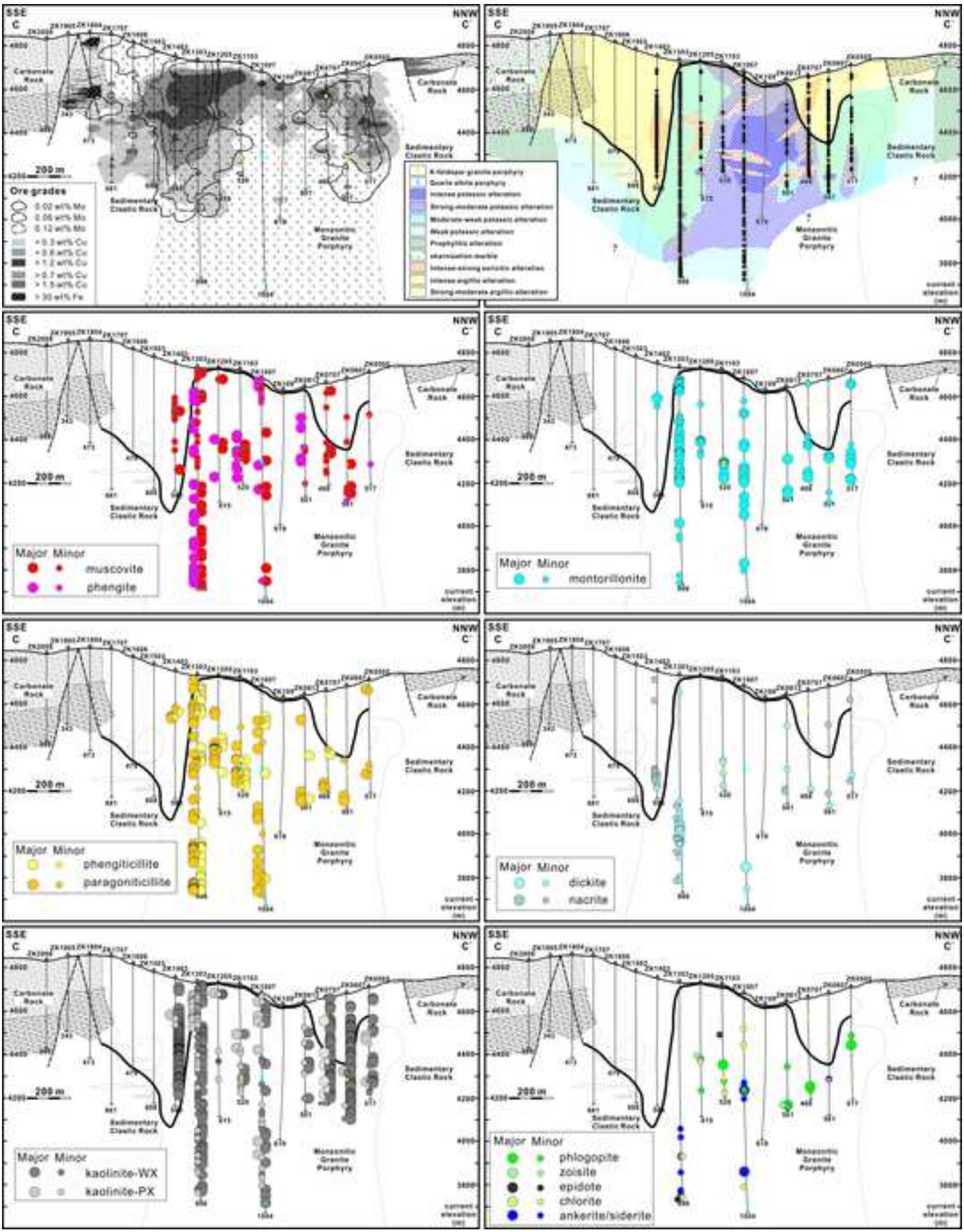

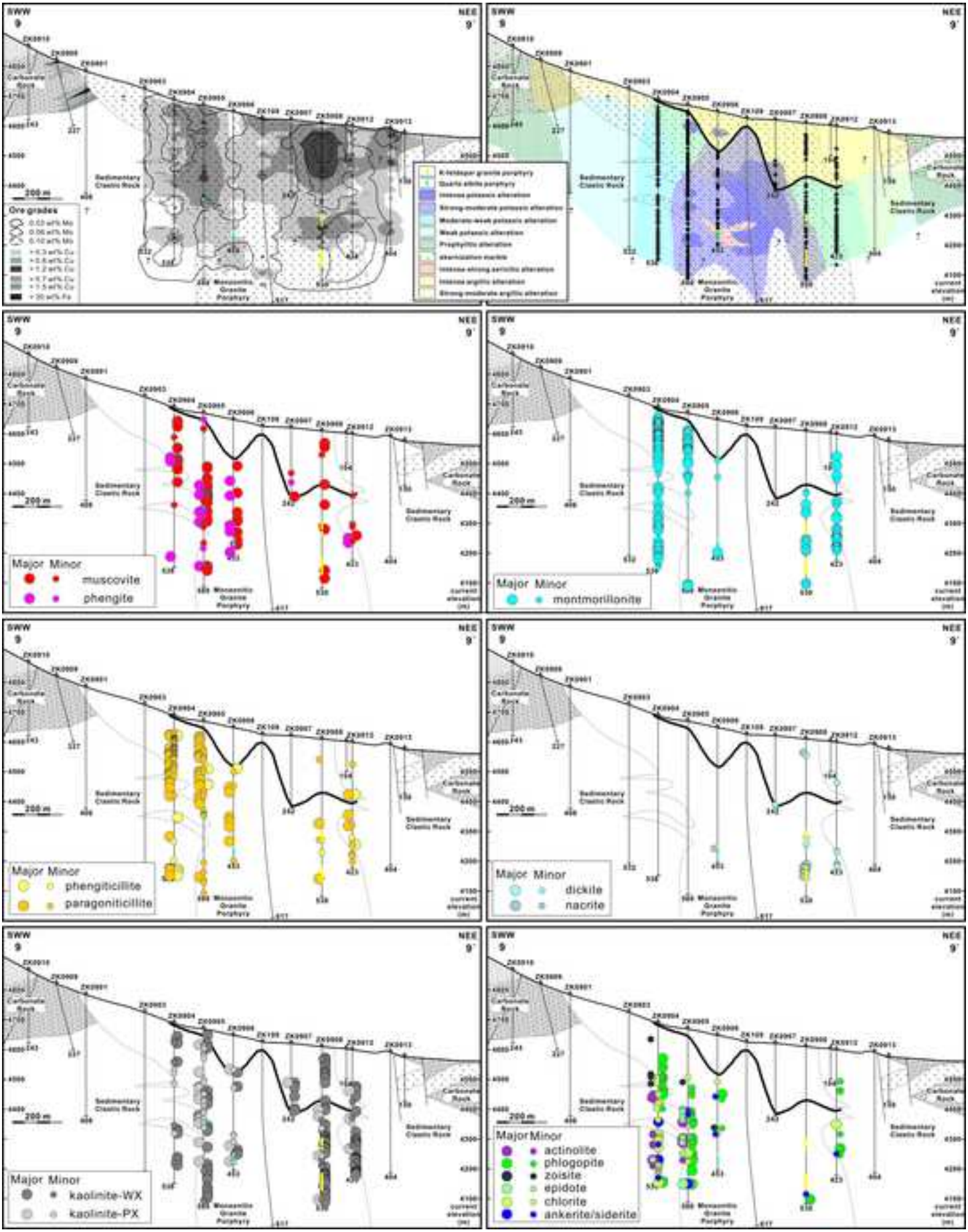

TABLE 1. Mineralogical Characteristics of Yulong Porphyry Rock Types

	Phenocryst vol.% and size range					Groundmass vol.%; main components and grain size
	K-feldspar	Plagioclase	Quartz	Biotite	Hornblende	
MGP	10-15% 5-30 mm	25-35% 0.5-8 mm	1-5% 1-5 mm	2-5% 0.5-3 mm	1-5% 0.5-5 mm	50-60%; qtz, ksp, plag, 0.01-0.2 mm
KGP[†]	2-3% 2-10 mm	10-25% (?) 0.5-4 mm	3-7% 1-2 mm	1-3% 0.25-1 mm	Rare	70-80%; ksp, qtz, 0.05-0.1 mm
QAP	1-2% 3-10 mm	10-15% 0.5-6 mm	1-2% 1-5 mm	3-7% 0.25-2 mm	Rare	80-85% qtz, ksp, plag, bio, 0.01-0.05 mm

Abbreviations: qtz = quartz, ksp = K-feldspar, plag = plagioclase, bio = biotite

[†]Mineralogical proportion estimated from moderately potassic altered rocks

TABLE 2. Paragenetic Sequence of Vein Types at the Yulong Porphyry Cu-Mo Deposit

Vein types	Vein textures	Thickness	Gangue minerals	Opaque minerals	alteration halos	distribution and Timing
Early stage veins (MGP →KGP)						
M_E veins	commonly lack definitive walls; irregular internal structure	1-8 mm	Major: qtz, bio, ksp Minor: act, rt, di, ank	Major: mt	some with mt-bio-ksp halos	Rarely occurring at deep level beneath the ore zone; cut by EB_E, A_E, B_T, and D_L veins
EB_E veins	irregular or straight walls; granular vein qtz intergrown with disseminated bio	0.5-10 mm	Major: qtz, bio Minor: rt, ap	none or overprinted by cp, py, mo	_	Few but common throughout the deposit; mostly cut by $A1_E$, $A2_E$, $A3_E$, B_T and D_L veins, also cutting some $A1_E$ and $A2_E$ veins
$A1_E$ veins	irregular or straight walls; ksp and trace bio occurring as dessiminates in qtz	5 mm->1 m	Major: qtz, ksp Minor: bio, rt, anh	none or overprinted by cp, py, mo	mostly absent; locally with narrow ksp halos	Dominat vein type in the barren core; cutting most of M_E and EB_E veins, cut by EB_E, $A2_E$, $A3_E$, B_T, and D_L veins
$A2_E$ veins	straight walls with anhedral, fine granular qtz; mo, cp, and py as disseminates or aggregates in qtz	1-30 mm	Major: qtz Minor: ksp, bio, ap, rt, anh	Major: mo, mo-cp ± py, cp-py	_	Dominat vein type in the shallow ore zone, associated with $A3_E$ veins; cutting EB_E and $A1_E$ veins, cut by EB_E, $A3_E$, B_T, and D_L veins
$A3_E$ veins	cp ± py-dominated with minor euhedral qtz	0.1-8 mm	Minor: qtz, ksp, bio	Major: cp ± py Minor: mo	_	Dominant vein type in the shallow ore zone, closely associated with $A2_E$ veins; cutting EB_E, $A1_E$, and $A2_E$ veins, cut by B_T veins
Transitional stage veins (KGP →QAP)						
UST_T	qtz layers much thiner than the inteval KGP	_	Major: qtz Minor: ksp	_	_	Occurring in the KGP close to the contact zone with the MGP; cut by $A1_T$ and B_T veins
EB_T veins	capillary bio-qtz veinlets	0.2-2 mm	Major: bio, qtz Minor: rt	_	_	Rarely observed in the KGP; cut by $A1_T$ veins
$A1_T$ veins	vein with irregular or straight walls, fine granular vein qtz	5-30 mm	Major: qtz Minor: ksp, bio, ap, rt, anh	_	_	In the KGP; cut by B_T veins
B_T veins	typical parallel "cockscomb" qtz; mo abundant in vein margins	1-10 mm	Major: qtz Minor: rt, anh, ank	Major: mo Minor: cp ± py	none or locally with sericitic halos	Commonly occurring in the deep Mo-rich zone; cutting all the vein types above
$A3_T$ veins	cp ± py-dominated; trace qtz	0.1-3 mm	Minor: qtz	Major: cp ± py	_	Rarely observed in the KGP; cutting $A1_T$ veins
Late stage veins (QAP →)						
D_L veins	straight-walled, euhedral qtz; more py than qtz in vein	1-10 mm	Major: qtz, ser Minor: cal, rt, fl	Major: py Minor: cp, gn, tn	commonly with sericitic halos	Abundant throughout the deposit; cutting all the other vein types

Abbreviations: bio = biotite, ksp = K-feldspar, qtz = quartz, act = actinolite, rt = rutile, di = diopside, mt = magnetite, ap = apatite, cp = chalcopyrite, py = pyrite, anh = anhydrite, mo = molybdenite, ank = ankerite, ser = sericite, cal = calcite, fl = flourite, gn = galena, tn = tennantite.

TABLE 3. Re-Os Data Synopsis for Molybdenite from the Yulong Porphyry Cu-Mo Deposit

Sample no. and location[1]	Brief sample description[2]	Grain size (mm)	Weight (g)	Re (ppm)	±	^{187}Re (ppm)	±	^{187}Os (ppb)	±	Model age (Ma)[3]	± (Ma)[4]
Early stage $A2_E$ veins											
1303-390	$A2_E$ vein in MGP (P-IA)	<0.1-1	0.010	127.13	0.65	79.90	0.41	56.30	0.27	42.28	0.17 (0.22)
0705-155	$A2_E$ vein in MGP (P-K)	0.1-1	0.010	435.72	2.26	273.86	1.42	190.66	0.92	41.77	0.17 (0.21)
1303-484	$A2_E$ vein in MGP (P-IA)	0.1-0.5	0.010	307.76	1.54	193.44	0.97	134.02	0.62	41.57	0.17 (0.21)
1303-114	$A2_E$ vein in MGP (P-IA-K)	<0.5	0.011	525.70	2.58	330.41	1.62	228.89	1.03	41.57	0.17 (0.21)
1303-256	$A2_E$ vein in MGP (P-S-K)	0.1-1	0.010	277.63	1.39	174.49	0.87	120.58	0.56	41.46	0.17 (0.21)
Transitional stage B_T veins											
0905-159	$A2_E$ vein refilled by B_T vein in MGP (P-IA)	0.5-2	0.010	144.65	0.73	90.92	0.46	62.04	0.29	40.95	0.17 (0.21)
1007-266	B_T vein in MGP (P)	0.1-0.5	0.010	167.18	0.84	105.07	0.53	71.67	0.33	40.93	0.17 (0.21)
0707-138	B_T vein in MGP (P-K)	0.5-2	0.011	139.69	0.69	87.80	0.43	59.90	0.27	40.94	0.17 (0.21)
1303-955	B_T vein in MGP (P?-S)	0.1-0.5	0.020	17.98	0.08	11.30	0.05	7.72	0.03	40.98	0.23 (0.26)
1103-497	B_T vein with sericitic halos in MGP (P-S)	< 0.1-0.5	0.010	74.81	0.38	47.02	0.24	32.09	0.15	40.95	0.17 (0.21)
0908-340	B_T vein in KGP (P?-K)	~0.2	0.010	156.71	0.78	98.49	0.49	67.18	0.31	40.92	0.17 (0.21)
0908-468	B_T vein with sericitic halos in KGP (P?-S)	0.2-0.5	0.010	276.78	1.40	173.96	0.88	118.75	0.55	40.96	0.16 (0.21)
1303-405	B_T vein in MGP (P-S)	0.1-1	0.010	61.13	0.31	38.42	0.20	25.33	0.12	39.56	0.17 (0.21)
0505-455	B_T vein in hornfels (P?-S)	0.1-1	0.011	108.37	0.54	68.11	0.34	42.17	0.19	37.15	0.15 (0.19)
Control sample											
RM8599	Molybdenite reference material		0.100	11.14	0.04	7.00	0.02	3.23	0.01	27.65	0.11 (0.13)

[1]Sample no. is named after sample location, for example, 1303-390 represents 390 m in drill hole ZK1303

[2]Abbreviations in parentheses represent the inferred alteration sequence of the $A2_E/B_T$ vein-hosting rocks. P: potassic alteration; IA: intermediate argillic alteration; S: sericitic alteration; K: supergene kaolinite alteration

[3]Ages calculated using $^{187}Os = {}^{187}Re\,(e^{\lambda t}-1)$; decay constant ($\lambda$) used for ^{187}Re is $1.666\times10\text{-}11$ year^{-1} (± 0.31%, Smoliar et al., 1996)

[4]Data are presented without and with (bracketed value) ^{187}Re decay constant uncertainty (Smoliar et al., 1996; Selby et al., 2007)

Click here to access/download

Electronic Appendix (Excel etc.)

Appendix 1 Short wavelength infrared spectral analysis.doc

Electronic Appendix (Excel etc.)

Appendix 2 LA-ICP-MS zircon U-Pb data of porphyry intrusions.xls